

Non-gravitational heating in the hierarchical formation of galaxies and X-ray clusters

K. K. S. Wu,^{1,3} A. C. Fabian¹ and P. E. J. Nulsen²

¹ *Institute of Astronomy, Madingley Road, Cambridge CB3 0HA*

² *Department of Physics, University of Wollongong, Wollongong NSW 2522, Australia*

³ *kwu@ast.cam.ac.uk*

ABSTRACT

The strong deviation in the properties of X-ray clusters from simple scaling laws highlights the importance of non-gravitational heating and cooling processes in the evolution of proto-cluster gas. We investigate this from two directions: by finding the amount of ‘excess energy’ required in intra-cluster gas in order to reproduce the observed X-ray cluster properties, and by studying the excess energies obtained from supernovae in a semi-analytic model of galaxy formation. Using the insights obtained from the model, we then critically discuss possible ways of achieving the high excess specific energies required in clusters. These include heating by supernovae and active galactic nuclei, the role of entropy, and the effect of removing gas through radiative cooling.

Our model self-consistently follows the production of excess energy as well as its effect on star formation in galaxies. Excess energy is retained in gas as gravitational, kinetic and/or thermal energy, especially if the gas is ejected from a galaxy—its low density then prevents further radiative loss. The gas distribution of virialized halos are modelled with a 2-parameter family of gas density profiles; gas profiles are then chosen according to the total energy of the gas. Our principle assumption is that in the absence of non-gravitational processes, the total energy of the gas scales as the gravitational energy of the virialized halo—a simple scaling law motivated by hydrodynamic simulations. We normalize this relation by matching the model to the largest observed clusters. We investigate four contrasting ways of modifying gas density profiles in the presence of excess energy, in order to study the sensitivity of results to the model. In addition, we estimate the minimum excess specific energy required when all available gas profiles are considered, using a fiducial cluster with a temperature of around 2 keV. We find that the excess specific energies required in clusters lie roughly in the range 1–3 keV/particle, with about 2 keV/particle being the most plausible.

The metal abundances of cluster gas suggest that it may be possible for supernovae to provide the required excess energy. However, if this energy is completely due to supernova heating, then a highly contrived model is required in which galaxies need to eject gas at specific energies of ~ 10 –100 times the binding energy of their halo. In this case, the role of supernovae as regulators of star formation is also significantly diminished.

Key words: galaxies: clusters: general – galaxies: formation – galaxies: evolution – cooling flows – X-rays: galaxies

1 INTRODUCTION

N-body simulations of the hierarchical clustering of non-baryonic dark matter (DM) now provide perhaps the best understood piece in the jigsaw of how galaxies formed and evolved. However, the evolution of the baryonic component, in particular the formation of stars and active galactic nuclei (AGN) in galaxies and the energy feedback which ensued, remain much less well understood. In both hydrodynamic simulations and semi-analytic models (SAMs) of galaxy formation on a cosmological scale, gas processes such

as star formation and supernova feedback have to be approximated by simple rules. Often this is simply due to the lack of more detailed knowledge, or it may be due to a lack of numerical resolution on small scales. Nevertheless, the simplicity of the rules allow the range of behaviour in the system to be easily explored and indeed allow predictions to be made. In this way, SAMs have achieved notable success in modelling many properties of galaxies (White & Frenk 1991; Kauffmann, White, & Guiderdoni 1993; Cole et al. 1994; Kauffmann & Charlot 1998; Baugh et al. 1998; Somerville & Primack 1998; Guiderdoni et al. 1998).

All SAMs of galaxy formation have a ‘skeleton’ which is given by the merger tree. The merger tree follows the masses of virialized halos with time. Individual halos increase in mass by merging with other halos or by accreting uncollapsed material. Whenever a ‘major merger’ occurs, a new halo is deemed to virialize. The new halo is given gas and DM density profiles, which allow the estimation of basic quantities such as the cooling time of the gas and the free-fall time. From this starting point, the model proceeds to estimate the rate of star formation, supernova feedback, metal enrichment and other quantities that can be compared with observations. At the next merger, the properties of the progenitor halos (e.g. the mass of gas remaining) are then incorporated into the new halo. By using many ‘realisations’ of such merger trees in a Monte-Carlo simulation, statistics on galaxy and cluster properties can be built up.

In this paper we investigate the effect of non-gravitational heating on the gas density profiles of halos and thus on the properties of galaxies and X-ray clusters. By non-gravitational heating we include heating by supernovae and AGN. The total energy released by such sources, when averaged over all baryons, comes to several keV per particle. It therefore has the potential to strongly influence the properties of X-ray clusters and galaxies. However, this may not be the case if most of the energy is radiated at some point.

Gas that is heated is able to retain the ‘excess energy’ as thermal, gravitational and possibly kinetic energy as it passes through the merger tree. Even if the gas is ejected from a halo, it is expected to recollapse later into a larger halo, thus the excess energy is not lost. In our model, gas that is ejected rejoins the halo at its next ‘major merger’. (Major mergers in our model result in halos that are at least twice the mass of any progenitor halo.) In this way, the excess energy in any gas halo is the result of the contributions from all the progenitor halos beneath it in the merger tree, after taking account of radiative cooling.

In order to model the effect of excess energy on gas halos, it is necessary to have a continuous range of gas profiles to choose from. The gas profile with density proportional to r^{-2} has been used successfully in many SAMs to model galaxies. However, it is too simple for modelling the properties of X-ray clusters. In particular, the core of the gas density profile has to be flattened in order to obtain results that match the data (Wu, Fabian & Nulsen 1998; WFN98). In WFN98 we introduced a family of isothermal gas profiles into our SAM. We assumed the gas to be in hydrostatic equilibrium inside potential wells given by Navarro, Frenk & White (1997; NFW97) density profiles. This family of gas profiles enabled us to increase the temperature of a gas halo uniformly, according to the excess energy in the gas. The main results from that paper are that we were able to fit the observed properties of X-ray clusters, including their gas fractions, metallicities, X-ray luminosity-temperature relation, temperature function, X-ray luminosity function and mass-deposition-rate function, by including excess energies of ~ 1 keV/particle.

The gas halos of clusters are well-known not to be ‘self-similar’, in the sense that small clusters (with temperatures $\approx 2 \times 10^7$ K) are not simply scaled-down versions of large clusters ($T \sim 10^8$ K), with the gas fraction kept the same. The X-ray luminosities of small clusters are an order of magnitude less than predicted by scaling down the luminosities of large clusters in this way. This suggests that the gas distributions of small clusters are more extended. However, hydrodynamic simulations without non-gravitational heating or cooling (e.g. Navarro, Frenk & White 1995) obtain X-ray clusters that are self-similar to a good approximation. In order to break the self-similarity of X-ray clus-

ters, excess energy is generally required. Excess energy can make the gas distribution more extended or even remove some gas from the halo. Different models for heating clusters and breaking their self-similarity have been studied by Kaiser (1991, Evrard & Henry (1991, Metzler & Evrard (1994, Navarro, Frenk, & White (1995, Cavaliere, Menci, & Tozzi (1997, Ponman, Cannon, & Navarro (1999, Balogh, Babul, & Patton (1999, Loewenstein (1999).

We have extended the family of gas profiles used in WFN98 by requiring that gas halos obey polytropic equations of state: $P \propto \rho_g^\gamma$, where P is pressure and ρ_g is gas density. This means that given the mass of gas in the halo and the shape of the potential well, the gas profile has two degrees of freedom in the model, given by the parameters: γ , which in effect gives the shape of the temperature profile, and η_{200} , which gives the normalization of the temperature profile. The isothermal profiles used in WFN98 are retrieved with $\gamma = 1$, while progressively steeper temperature gradients are obtained by increasing γ . We thus have the choice of increasing the temperature of a gas halo uniformly with radius or preferentially towards the centre, depending on the ‘heating model’ that is used. One of the main purposes of this paper is to determine the level of excess energy that intra-cluster gas must have in order to match the observed properties of X-ray clusters. We then critically discuss possible ways of obtaining this level of heating.

The SAM used in this paper is based on that described by Nulsen & Fabian (1997, 1995; NF97 and NF95). A discussion of the main areas of difference with other SAMs is given in NF97. The differences between SAMs demonstrate that, at present, the observed data can frequently be explained by a variety of models, testifying to the complex origin of what we observe. Eventually, one expects the different models to converge. We emphasize that our analysis of the excess energies required in X-ray clusters is not affected by such differences, as their X-ray properties depend almost entirely on their gas profiles only.

We assume the same cosmology and density fluctuation spectrum throughout. The cosmological parameters are $H_0 = 50$ km s $^{-1}$ Mpc $^{-1}$ and $\Omega_0 = 0.3$, with no cosmological constant. A cold dark matter (CDM) power spectrum of density fluctuations is used, with a primordial spectral index of $n = 1$ and normalized to give $\sigma_8 = 0.75$. We use a baryon density parameter of $\Omega_b = 0.08$, as suggested by big-bang nucleosynthesis and deuterium abundance measurements, which give $\Omega_b = 0.02h^{-2}$, where $H_0 = 100h$ km s $^{-1}$ Mpc $^{-1}$ (Burles & Tytler 1998; Burles et al. 1999). This implies that the initial gas fraction is equal to 0.27.

1.1 Plan of the paper

We give a full description of our SAM in sections 2 to 4, supplemented by technical details which are given in Appendix A. As with the merger tree, the gas and DM profiles of halos form the starting point of any SAM. Hence, it is possible and indeed useful to describe the modelling of gas processes independently of the gas and DM profiles assumed. This is done in section 2. In section 3 we describe the density profiles of NFW97, which we use to describe the total density distributions of halos. This leads to a formula for the potential wells of halos. By assuming a polytropic equation of state, we are then able to derive a 2-parameter family of gas profiles in section 4.1.

We begin section 4 by explaining why we use the total specific energy, E_{gas} , to select the gas profiles of *all* halos (including those without excess energy) and describe how this is done. We define what we mean by the ‘default profile’ of a given halo and explain

what constitutes a ‘heating model’. In section 4.1 we derive the family of gas profiles and plot examples to illustrate the effect of heating. Finally, we present four specific heating models in section 4.2 and explain how they are calibrated to match the largest observed clusters. In Appendix A we give the equations used in the model (as described in section 2) and apply them to the family of gas profiles.

In section 5 we set the free parameters of the SAM, in particular ϵ_{SN} which controls the efficiency of supernova energy injection and τ_0 which determines whether a collapse results in cold gas or a hot hydrostatic atmosphere.

In section 6 we investigate the role of supernova heating by first obtaining the excess energies that result in the halos of dwarf galaxies through to clusters. Using two different heating models, we show that the result obtained is generic. We then discuss the effect of the excess energies on the amount of star formation in ‘normal’ galaxies.

In section 7 we find the excess energies required in intra-cluster gas in order to fit the observed X-ray luminosity-temperature relation. To investigate the uncertainty in the energy required, this is repeated for all four heating models. The resulting fits to other X-ray data are presented. We end by calculating the minimum excess energy required in a small cluster of about $10^{14} M_{\odot}$, given the full set of gas profiles to choose from.

In section 8 we discuss some other effects which may contribute to the excess energy, but which are not included in our model. In the process, we give a more formal definition of excess energy and discuss the theory behind the concept in some detail.

Finally, in section 9 we discuss four possible scenarios for breaking the self-similarity of clusters, aiming to be as model-independent as possible. We consider three sources of excess energy: supernovae, AGN and the selective removal of gas by cooling. We also discuss the role of entropy in this problem (section 9.2). We emphasize that both energy and entropy are important in determining the final gas distribution. Our conclusions are summarized in section 10.

2 BRIEF DESCRIPTION OF THE MODEL

We begin with a general description of our model which can be applied to any reasonable gas and DM halo profiles. More detailed discussions of the gas processes can be found in NF95 and NF97, which assumed essentially the same physics as used here. In Appendix A we apply the rules given in this section to the set of density profiles that we shall adopt.

2.1 Merger trees

Merger trees of virialized halos are simulated using the Cole & Kaiser (1988) block model. In a ‘complete’ simulation, we use 20 levels of collapse hierarchy where the smallest regions are $1.5 \times 10^{10} M_{\odot}$ in mass. In the block model, masses increase by factors of 2 between levels, so that the mass of the largest block is $7.9 \times 10^{15} M_{\odot}$. This allows us to simulate the full range of structures from dwarf galaxies to the largest present-day clusters. However, if we are considering X-ray cluster properties only, it is ~ 1000 times faster to simulate only the top 10 levels of the collapse tree. The mass of the smallest regions is then $2^{10} \times 1.5 \times 10^{10} = 1.5 \times 10^{13} M_{\odot}$. In such low-resolution simulations some additional assumptions need to be made, such as the value of the gas fraction left over from the formation of galaxies.

Since every collapse of a block (which corresponds to a major infall or merger) at least doubles the mass of the largest progenitor halo, a new halo is said to virialize with each collapse. The virial radius, r_{200} , is defined such that the mean density within it is 200 times the background density of an Einstein-de Sitter universe of the same age. The total mass of the halo inside r_{200} is equal to the mass of the collapsed block. Likewise, the gas mass inside r_{200} is the contribution from the entire block. A collapse which is followed too closely by a larger-scale collapse does not have time to form a virialized halo. It is therefore not counted as a separate collapse. We allow a minimum time interval between collapses which is parametrized as a multiple of the dynamical time. Our results are not sensitive to this parameter and it is given a value of 1.

2.2 Cold and hot collapses

Once the halo has virialized, the remaining physics is concerned solely with the gas, within our approximation. For a gas halo to be considered hydrostatic, the gas at any radius has to remain still for at least the time it takes for sound to travel to the centre, which can itself be approximated by the free-fall time. As discussed in NF95, when the ratio of the cooling time to the free-fall time to the centre, $\tau = t_{\text{cool}}/t_{\text{ff}}$, is less than ~ 1 , then the gas cools fast enough that it is not hydrostatically supported. It fragments and collects into cold clouds which we assume to form stars with a standard or slightly modified initial mass function (IMF). We refer to this as a cold collapse and the gas that takes part in it as cold gas.

The criterion above can also be understood as follows: shocks produced in a collapse tend to work outwards from the centre, with the pressure of shocked gas effectively giving the working surface on which more gas gets shocked. If $\tau \lesssim 1$ then this working ‘surface’ is broken up or non-existent. Thus although infalling gas may still shock, it is not supported by pressure and remains very clumpy.

When $\tau \gtrsim 1$, a hydrostatic atmosphere of hot gas (at roughly the virial temperature) is able to form. In this case, a cooling flow occurs if some gas has time to cool before the next collapse. Cooling gas flows inward subsonically and remains hydrostatically supported. Cooling flows are common in clusters of galaxies (Fabian 1994) and observations show that the gas that cools does not form stars with a standard IMF but must remain as very small, cold clouds or form low-mass stars. We refer to the product simply as baryonic dark matter (BDM).

To estimate the masses of hot and cold gas produced in a collapse, we use the gas and total density profiles to estimate t_{cool} and t_{ff} as functions of radius. To simplify computation, t_{ff} is estimated using the free-fall time of a test particle in a uniform background density, i.e. $t_{\text{ff}} = \sqrt{3\pi/16G\rho}$, where G is the gravitational constant and the total density at the radius concerned is substituted for ρ . (This gives a slight overestimate, as density actually increases towards the centre.) We thus obtain $\tau(r)$ and compare it to a critical value, τ_0 . In well-behaved cases τ increases monotonically with radius, so that there exists at most one radius where $\tau = \tau_0$, inside of which gas is labelled as cold, and outside, as hot. We call this radius r_{CF} . If τ is greater than or less than τ_0 throughout the halo, then r_{CF} is made equal to 0 or r_{200} , respectively. As halo mass increases, the trend is for r_{CF} to move from the virial radius to the centre. In other words, cold collapse gives way to hot collapse as we go to larger halos. This transition is quite abrupt and takes place over about one decade in mass.

From above, it is clear that no single gas profile can always describe the gas halo. Cooling modifies the gas distribution, and

in a cold collapse the assumption of hydrostatic equilibrium breaks down completely. However, the gas profile used in the model is only *notional*—defined as that obtained in a notional collapse with cooling ignored (Nulsen, Barcons & Fabian 1998). Used in this way, it allows us to estimate the behaviour of different subsets of gas. In the case of hot halos, if the part that has cooled is small compared to the whole, then the density and temperature of gas away from the cooled region do not change significantly as the halo reestablishes hydrostatic equilibrium. The original gas profile therefore gives reasonable estimates of bulk properties.

2.2.1 The criterion when excess energy is large

If the excess energy from heating is large enough to be comparable to the binding energy of the gas halo (as defined in section 4), then τ may not increase monotonically with radius. Examples of this are shown in Appendix A. Such cases can account for a fair fraction of dwarf and small normal galaxies because of their smaller binding energies. This raises the question of whether gas with $\tau < \tau_0$ *outside* a core of gas where $\tau > \tau_0$ still ends up cold after collapse. Since the value of τ and its interpretation are approximate, we opt for a simple criterion in such cases, which determines whether all or none of the gas halo takes part in a cooling flow (Appendix A). We note that $\tau(r)$ is a fairly flat function of radius in such cases, if only isothermal gas profiles are used.

2.3 Star formation, supernova feedback and cooling flows

Star formation is presumed to proceed rapidly in the cold gas and leads quickly to type II supernovae. This is assumed to continue until the energy from supernovae is sufficient to eject the remaining gas in the halo to infinity, or until the cold gas is used up. If the gas halo is not ejected, supernova energy can modify the gas density profile by increasing the total energy of the remaining gas (section 4). The effect of this is generally small but is included for consistency. The remaining gas, which is hot, may then take part in a cooling flow, depositing BDM if it manages to cool by the next collapse or the present day. For halos which contain only hot gas or cold gas, the situation is naturally simpler than described.

We only follow the production of type II supernovae (SNII) in our model. Precise knowledge of the IMF is not required, as we only need to know the number of SNII resulting from a certain amount of star formation. It is generally assumed that the progenitors of SNII are stars with $M > 8M_\odot$. For a Miller-Scalo IMF, we adopt the estimate of one SNII for every $80M_\odot$ of stars formed with $M \leq 1M_\odot$ (Thomas & Fabian 1990), where M is the stellar mass. In section 5, we shall require the mass of stars remaining in clusters today to be a certain fraction of the gas mass. Since the lifetime of a star is approximately $10^{10} (M/M_\odot)^{-3}$ years, the above range of M results in a good approximation of the stellar mass remaining in a cluster today.

In the simulations, we assume instantaneous recycling of stars with $M > 1M_\odot$. In reality, stars of intermediate mass ($1M_\odot < M < 8M_\odot$) recycle their gas as planetary nebulae on intermediate time scales. However, the effect of this simplification is small, because the stellar mass in a halo is almost always $\lesssim 1/10$ of the gas mass (an exception occurs in halos of a few $10^{12}M_\odot$, where a quarter to a half of halos have more stars than this at the beginning of a collapse stage). Thus the gas mass in any halo is little affected by recycling. As for the stellar mass, we shall only require precise values in present-day clusters. The above simplification does

not affect the amount of star formation in halos that contain only cold gas, because the fraction of cold gas that forms stars is then $\lesssim 1/10$. However, an ambiguity arises when a large fraction (close to 1) of the cold gas forms stars. This can occur if the cold gas is only a fraction of all the gas in the halo. In this case, the assumption of instantaneous recycling can lead to an overestimate of the amount of star formation (as the estimated mass of stars formed with $M < 1M_\odot$ may be as large as the mass of all the cold gas available). Fortunately, the fraction of stars formed in this way is very small, so that the resulting error in the stellar mass of present-day clusters is less than 1 per cent.

In the simulations, we follow NF97 in boosting the above supernova rate by a factor of 5, which corresponds to flattening the slope of the IMF. Hence each SNII is associated with $16M_\odot$ of stars formed with $M < 1M_\odot$. Since the bulk of star formation in our model occurs in massive bursts in dwarf galaxies, it should not be surprising to find that the IMF is modified under such circumstances. For example, a power-law IMF with a slope of $x = 0.9$ (compared to the Salpeter IMF where $x = 1.35$), and lower and upper cutoffs of $0.1M_\odot$ and $50M_\odot$, gives 1 SNII for every $15M_\odot$ of stars with $M < 1M_\odot$. (Results are not very sensitive to the upper cutoff, because very massive stars are rare.) If the stars in a present-day cluster actually have half the age we have assumed, then we should include the mass of stars up to $M = 0.5^{-1/3} = 1.26M_\odot$. For the above IMF, the stellar mass in the range $0.1M_\odot < M < 1.26M_\odot$ is 11 per cent greater than that in the range $0.1M_\odot < M < 1M_\odot$. Hence this is the level of uncertainty in the stellar mass of clusters.

The energy per supernova available for the ejection of gas is parametrized as $4 \times 10^{50} \epsilon_{\text{SN}}$ erg. Each SNII is assumed to release $0.07M_\odot$ of iron (Renzini et al. 1993) and the solar iron abundance is taken to be 0.002 by mass (Allen 1976). Renzini et al. found the average iron yield to be fairly insensitive to the slope x of the IMF. A more recent compilation of average iron yields from a range of SNII models (Nagataki & Sato 1998) shows a wider dispersion, ranging from 0.07 to $0.14M_\odot$ of iron per SNII. However, most of the SNII models assume solar metallicity for progenitor stars, whereas the bulk of star formation in our model occurs in low metallicity dwarf galaxies. If only low metallicity SNII models are included, then the range narrows to about $0.07\text{--}0.09M_\odot$ of iron per SNII.

The excess energy of a gas halo in the model is given by the effects of supernova heating and radiative cooling integrated over the history of the gas. At each collapse, the average iron abundance and excess energy of the gas are found and incorporated into the new gas halo.

2.4 Classification of galaxies

We assume that the transition from cold to hot collapse also corresponds to the transition from dwarf to normal galaxies (NF97). Thus halos that deposit more mass in stars than BDM in a given collapse are identified as dwarf galaxies. Dwarf galaxies are assumed to become disrupted in the next collapse, thus losing their identities. If instead more mass is deposited in BDM than stars in the collapse, then a normal galaxy is created (assuming none existed in the halo to begin with). We consider the dissipation that occurs in cooling flows to be an important factor in the survival of normal galaxies during halo mergers. Thus normal galaxies retain their identities through subsequent collapses. If one or more normal galaxies exist at the start of a collapse stage, then one is considered to reside at the centre of the halo, becoming the site of any new star formation. Halos that contain more than one normal galaxy are

identified as groups and clusters (which have the same meaning in the model).

In this paper, we shall only require the morphologies of normal galaxies in the field, i.e. those that do not occur in groups. A simple criterion is used to determine the morphology of a normal galaxy. If all of the hot gas in a halo manages to cool, then the last gas to cool is argued to rotate rapidly and thus forms a disc (NF97, Fabian & Nulsen 1994). A normal galaxy occurring alone in such a halo (possibly created in the same collapse) is thus identified as a spiral galaxy. All other normal galaxies are identified as ellipticals. An elliptical may therefore be converted into a spiral, but there is no mechanism for converting a spiral into an elliptical. We do not follow disc star formation in the present model. We note that the above mechanism for creating spiral galaxies may explain why X-ray luminous gas halos have not been detected around spiral galaxies, contrary to the predictions of other SAMs of galaxy formation (Benson et al. 1999).

3 THE DISTRIBUTION OF TOTAL DENSITY IN HALOS

We begin by specifying the total density profile of a halo, which allows us to derive the shape of the potential well. This is then used in the following section to derive gas density profiles.

From a series of dark matter simulations in different cosmologies and with different density fluctuation spectra, Navarro, Frenk & White (1997; NFW97) found that the density profiles of virialized halos obeyed a universal form, given by

$$\rho(r) = \frac{\delta_c \rho_{\text{crit}}}{(r/r_s)(1 + r/r_s)^2}, \quad (1)$$

where r is the radius, r_s the scale radius and δ_c the characteristic density. We shall also use $x = r/r_s$ to denote the radius, and the value of x at the virial radius, $c = r_{200}/r_s$, is called the concentration. We take ρ_{crit} to be the density of an $\Omega = 1$ universe with age given by the time when the halo virialized (this is slightly different from NFW97, who used $\rho_{\text{crit}} = 3H^2/8\pi G$, where H is the Hubble parameter when the halo virialized). The mean density within r_{200} is required to be $200\rho_{\text{crit}}$, as motivated by the spherical collapse model. It follows that δ_c and c are related by,

$$\delta_c = \frac{200}{3} \frac{c^3}{[\ln(1+c) - c/(1+c)]}. \quad (2)$$

Hence given ρ_{crit} and the mass of the halo, there is only one free parameter, which may be expressed by c or δ_c . The Appendix of NFW97 gives a procedure for determining this parameter, which gave reasonable fits to simulated results. The method amounts to making the scale density, $\rho_s = \delta_c \rho_{\text{crit}}$, equal to 3000 times the background density when the halo was ‘assembled’, subject to an appropriate definition of this assembly time. The assembly time is a function of halo mass and redshift of virialization only (given the cosmology and fluctuation spectrum), hence the density profile is totally determined.

We make the further approximation that the NFW profile describes the total density in a halo (i.e. including the gas density) and that it is truncated to zero for $r > r_{200}$. This allows us to derive the gravitational potential as a function of x :

$$\phi(x) = \alpha \left(-\frac{\ln(1+x)}{x} + \frac{1}{1+c} \right), \quad (3)$$

where $\alpha = 4\pi G \rho_s r_s^2$.

Figure 1 shows a scatter plot of concentrations against halo

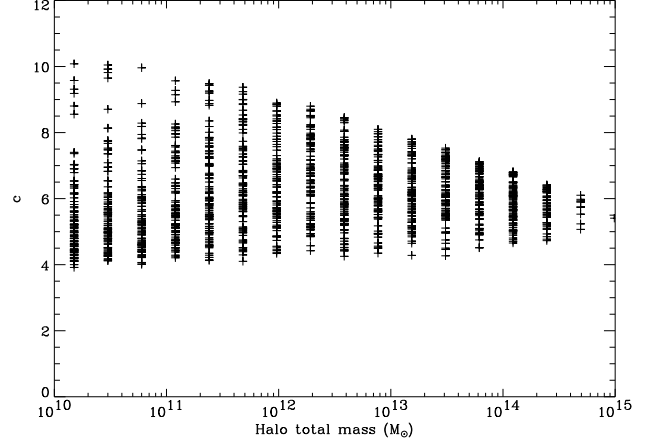


Figure 1. Scatter plot of c values vs. halo mass. Halo masses take discrete values in the block model. A maximum of 100 points per mass was used, in order to illustrate the density of occurrence. Note that this is a random sample of all halos that ever collapsed.

mass, to illustrate the values obtained for our choice of cosmology and fluctuation spectrum. For a fixed redshift of virialization, c increases substantially with decreasing mass. For example, halos that virialize at $z = 0$ occur along the top edge of the distribution, where c is found to range from roughly 6 to 10. In the distribution as a whole this is compensated by the tendency for small halos to virialize at higher redshift, because the value of c decreases with increasing redshift for a given mass.

4 THE DISTRIBUTION OF GAS IN HALOS

Given the shape of the potential well, $\phi(r)$, and the mass of gas in the halo, we make two further assumptions in order to calculate the gas density profile. The first assumption is that the gas is in hydrostatic equilibrium, i.e.

$$\frac{dP}{dr} = -\rho_g \frac{d\phi}{dr}, \quad (4)$$

where P is the gas pressure and ρ_g is the gas density, and the second is that P and ρ_g are related by a certain equation of state. For example, in WFN98 we assumed a perfect gas law and a constant temperature for the gas. In this case, $P \propto \rho_g$ and the only parameter that needs to be specified is the temperature, T . Once T is specified, the gas profile is uniquely determined. Below, we shall explain the general procedure that is used to determine such parameters.

Since we need to be able to vary the total energy of a gas halo according to the excess energy in the gas, we find it convenient to always use the total energy to constrain the parameter(s) of the gas profile, even when there is no excess energy. Thus we begin by specifying the total specific energy of a gas halo when there is no excess energy.

The total specific energy of a gas halo, E_{gas} , is the sum of thermal and gravitational terms:

$$E_{\text{gas}} \equiv \frac{1}{M_{\text{gas}}} \int \rho_g \left(\frac{3kT}{2\mu m_H} + \phi \right) dV, \quad (5)$$

where M_{gas} is the mass of gas in the halo and the integral is performed over the volume of the halo. The Boltzmann constant is denoted by k and μm_H is the mean mass per particle of the gas.

Thus for the gas halo to remain bound, we must have $E_{\text{gas}} < 0$. In the absence of excess energy, we postulate that E_{gas} is proportional to the specific gravitational energy of the whole halo. Thus

$$E_{\text{gas}} = K \frac{1}{M_{\text{tot}}} \int \frac{1}{2} \rho_{\text{tot}} \phi \, dV, \quad (6)$$

where ρ_{tot} is the total density (which follows the NFW profile), M_{tot} is the total mass of the halo and K is a constant which remains to be specified. In other words, we assume that the behaviour would be self-similar in the way expressed above if non-gravitational heating or cooling were not included. The value of E_{gas} then leads to a unique gas profile if there is only one parameter to determine, as in the example above. In general, a numerical procedure is needed to search for the gas profile with the matching value of E_{gas} .

For a given halo, the gas profile obtained in the absence of excess energy is called the *default profile*. We define the *binding energy* of the gas to be the magnitude of E_{gas} in this case. Thus the binding energy is unique for a given halo and may be regarded as the ‘default’ value of $|E_{\text{gas}}|$. The calibration of K is achieved by requiring that the default density profiles of the largest clusters approximate well those from X-ray observations. We match to the largest observed clusters because if heating does occur, we expect it to have least effect on them.

If the excess specific energy, E_{excess} , is non-zero, then we get

$$E_{\text{gas}} = K \frac{1}{M_{\text{tot}}} \int \frac{1}{2} \rho_{\text{tot}} \phi \, dV + E_{\text{excess}}. \quad (7)$$

If there is only one parameter to determine, then the gas profile is found in the same way as before. In general, as E_{excess} increases, the gas temperature increases and the density profile becomes flatter. Thus the excess energy goes into increasing both the thermal energy and the potential energy of the gas halo.

In the example above, the temperature increases uniformly with radius in the presence of heating, as the gas is always isothermal. Frequently, properties such as the luminosity of an X-ray cluster or the amount of gas that can cool in a given time are sensitive only to the gas density near the centre. Therefore if we increase the temperature preferentially towards the centre, then we can obtain the same changes in these properties for less excess energy. A convenient way of modelling non-isothermal profiles is to use a polytropic equation of state: $P \propto \rho_g^\gamma$. The parameter γ varies between 1 (resulting in constant temperature as before) and 5/3 (which gives an isentropic atmosphere). There are then two degrees of freedom, given by γ and the constant of proportionality in the polytropic equation. For the second parameter we shall use the temperature at the virial radius, T_{200} (or rather a dimensionless form of it). Since there are two parameters, a continuous range of gas profiles now have the same value of E_{gas} . Thus a further constraint is required to determine the gas profile uniquely.

A ‘heating model’ is obtained by specifying the constraint used to obtain the default profile and the path (in parameter space) followed by the gas profile as E_{excess} increases. The value of K used with the heating model also needs to be specified. Thus we essentially use a series of profiles to model the effect of heating. The choice of such a series is of course artificial. In reality, the gas distribution is determined by additional factors such as the gas entropy, how matter falls into the halo and how shock heating occurs. In lieu of such a complex model, we shall use a few contrasting heating models to see how sensitive our results are to the model.

4.1 A 2-parameter family of gas density profiles

We now derive the family of gas profiles used in our model, assuming a polytropic equation of state and a perfect gas law. If we first let $\gamma = 1$, implying a constant temperature T , then equation 4 gives

$$\rho_g(r) \propto \exp\left(-\frac{\mu m_H}{kT} \phi(r)\right). \quad (8)$$

Inserting the expression for the NFW potential (equation 3) yields

$$\rho_g(r) \propto (1+x)^{\eta/x}, \quad (9)$$

where $\eta = \mu m_H \alpha / (kT)$ is a dimensionless parameter that corresponds to the temperature and α is the characteristic gravitational potential of the NFW profile. By fitting the surface brightness profile obtained from this density distribution to large observed clusters, Ettori & Fabian (1998) found that the average value of η was around 10.

The isothermal profiles take a particularly simple form. For $\gamma \neq 1$, we use $P \propto \rho_g^\gamma$ to eliminate P in equation 4 and then use $\rho_g^{\gamma-1} \propto T$ to get

$$\frac{d}{dr} \left(\frac{kT}{\mu m_H} \right) = -\frac{\gamma-1}{\gamma} \frac{d\phi}{dr}. \quad (10)$$

Substituting for the potential now gives

$$\frac{T}{T_{200}} = 1 + \frac{\gamma-1}{\gamma} \eta_{200} \left(\frac{\ln(1+x)}{x} - \frac{\ln(1+c)}{c} \right), \quad (11)$$

where $\eta_{200} = \mu m_H \alpha / (kT_{200})$ is the value of η at r_{200} (where $x = c$). Thus using $\gamma > 1$ causes the temperature to increase monotonically towards the centre. Using $\rho_g \propto T^{(1/\gamma-1)}$, we get

$$\frac{\rho_g}{\rho_{g,200}} = \left[1 + \frac{\gamma-1}{\gamma} \eta_{200} \left(\frac{\ln(1+x)}{x} - \frac{\ln(1+c)}{c} \right) \right]^{\frac{1}{\gamma-1}}, \quad (12)$$

where $\rho_{g,200}$ is the gas density at r_{200} . It is straightforward to show that this approaches the isothermal form (9) as $\gamma \rightarrow 1$. We henceforth use the parameters γ and η_{200} to specify the gas profile.

It is also useful to calculate the ‘entropy’, $s = T/n_e^{2/3}$, where n_e is the electron density and $n_e \propto \rho_g$, which may be regarded as a label for the adiabat that the gas is on. For the gas to be stable to convection, the entropy must increase with radius. When $\gamma = 5/3$, the entropy is constant with radius and thus the atmosphere is marginally stable to convection. Atmospheres with higher values of γ and steeper temperature gradients convect to reduce the temperature gradient. Hence 5/3 is the maximum value of γ used in the model. The minimum value used is $\gamma = 1$. We have not used lower values of γ as there is little evidence for the temperature in a halo to increase with radius, both from X-ray cluster observations and hydrodynamic simulations.

In Figs. 2, 3 and 4 we display the density, temperature and entropy profiles, respectively, of a selection of gas halos which cover a range of η_{200} and γ values. All other parameters, in particular the total gas mass and the parameters of the NFW profile, have been kept constant. The series of dotted and dashed curves (in each figure) represent two different ways of heating the gas halo given by the solid curves. In each series, the value of E_{gas} has been required to increase at regular intervals between that of the solid curve and zero. Hence the gas halo with the most energy in each series is only marginally bound. It is evident from comparing the two series that profiles with the same total energy can differ significantly.

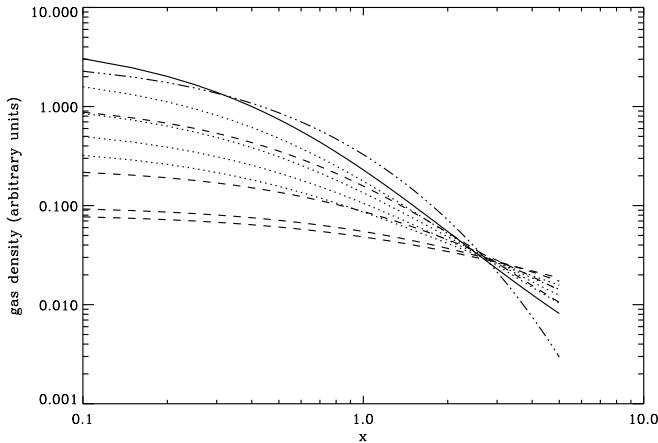


Figure 2. Gas density profiles, with parameters representative of those obtained in heating models A and B (see Fig. 5 and text). All parameters which pertain to the NFW profile are kept constant; in particular, $c = 5$. Each distribution is normalized to have the same total gas mass. The solid curve (the default profile for the purposes of this figure) uses $\eta_{200} = 10$ and $\gamma = 1$. The series of dotted profiles are obtained by decreasing η_{200} while keeping $\gamma = 1$ (Model B) and have the following parameters: $\eta_{200} = 8.5, 7.1, 6.0$ and 5.1 . They are chosen so that their total specific energies E_{gas} increase at regular intervals. The flattest curve, with $\eta_{200} = 5.1$, has zero total energy. Hence it is marginally bound. The series of dashed curves (corresponding to Model A) have the same total energies as the dotted curves, but have the following parameters: $(\eta_{200}, \gamma) = (10, 1.1), (10, 1.3), (8.7, 5/3)$ and $(6.8, 5/3)$. Notice that the same increases in total energy have more effect on densities at small radii if we increase γ rather than decrease η_{200} . Finally, the dot-dashed curve uses $\gamma = 1.2$ and $\eta_{200} = 28$, and is typical of default profiles obtained in Models C and D. Note how this curve roughly follows the solid curve, despite having a different shape (see Section 4.2 for discussion).

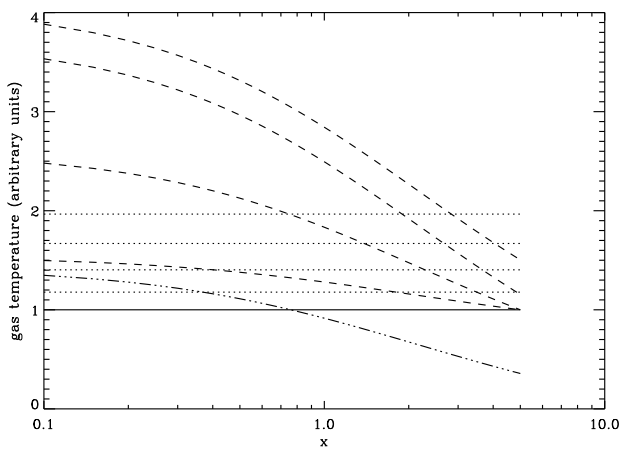


Figure 3. As Fig. 2, but showing temperature profiles. Note that temperature is plotted on a linear scale here. Temperatures have been normalized such that the temperature of the solid curve is unity. Increasing γ leads to steeper temperature gradients while keeping the temperature at the virial radius ($x = c$) constant. In contrast, decreasing η_{200} increases temperatures uniformly at all radii.

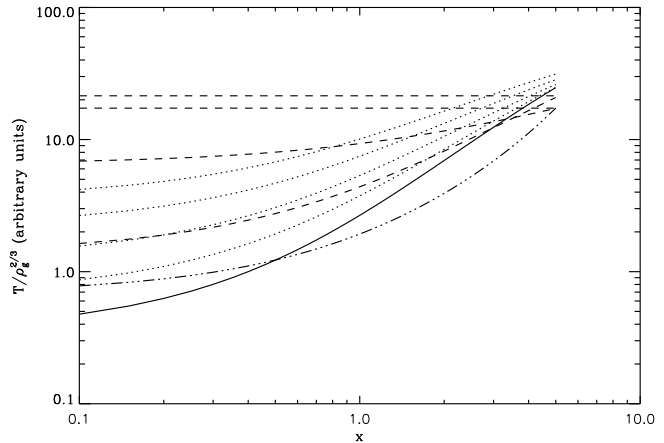


Figure 4. As Fig. 2, but showing entropy profiles. The ‘entropies’ were obtained by substituting the values plotted in Figs. 2 and 3 into the formula $T/\rho_g^{2/3}$. Most of the profiles are quite steep, but increasing γ (dashed curves) results in much flatter entropy profiles. Isentropic profiles are obtained when $\gamma = 5/3$.

4.2 Choosing profiles: the heating models

As discussed earlier, in addition to the value of E_{gas} one further constraint is required in order to specify a gas profile. We shall use two possible constraints for obtaining the *default* profiles of halos: $\gamma = 1$ or $\gamma = 1.2$, depending on the heating model. The former results in unheated gas halos that are isothermal and is motivated by its simplicity. The latter is motivated by the temperature profiles of X-ray clusters as measured by Markevitch et al. (1997), who approximated their results with a polytropic index of 1.2–1.3. For each of these cases, we need to calibrate the value of K used in equation 6.

We calibrate K by matching the model clusters obtained with $E_{\text{excess}} = 0$ to the largest observed clusters. We do not attempt to estimate K theoretically, as it is our opinion that E_{gas} depends upon how the collapse occurred in detail. For example, how the gas collapsed relative to the dark matter affects how much energy was transferred between the two components. However, we do assume that such processes result in the scaling law expressed in equation 6.

To calibrate K for the case of $\gamma = 1$, we use the results of Ettori & Fabian (1998), who studied the surface brightness profiles of 36 *ROSAT* PSPC clusters with X-ray luminosities of $L_X \gtrsim 10^{45}$ erg s $^{-1}$. When fitting to avoid any cooling flow region, they obtained a mean value of $\eta = 10.30$ with an rms deviation of 1.68. (Since the temperature is constant, η and η_{200} are the same.) In order to match this we set $K = 1.2$, which gives a mean value of $\eta = 10.5$ in the corresponding model clusters. However, our model does not reproduce such a large spread in η . When we also set the gas fraction of clusters to be 0.17 (the mean value measured by Evrard 1997 and Ettori & Fabian 1999, assuming $H_0 = 50$ km s $^{-1}$ Mpc $^{-1}$), we find that the model clusters naturally follow the observed X-ray luminosity-temperature ($L_X - T$) relation for clusters more luminous than 2×10^{45} erg s $^{-1}$ (Allen & Fabian 1998). (We refer to bolometric X-ray luminosities throughout.) Note that the fit is possible because the largest observed clusters roughly follow the self-similar relation $L_X \propto T^2$, instead of the steeper relation observed in smaller clusters.

Turning to the case of $\gamma = 1.2$, we first note that the surface brightness profiles of real clusters are almost always more closely

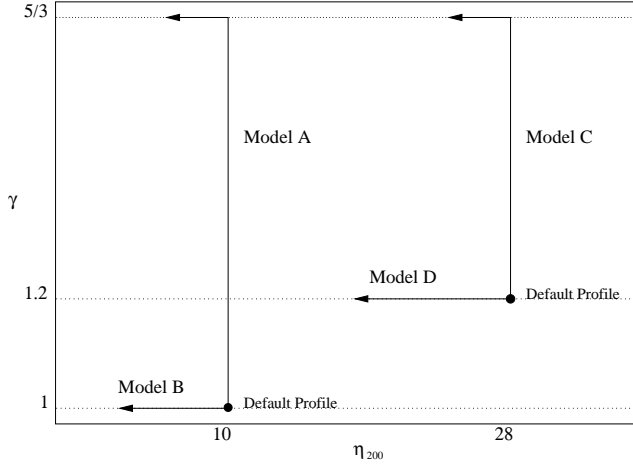


Figure 5. A schematic diagram of how one searches for gas profiles in each heating model. In general, it is necessary to first find the default gas profile, which has zero excess energy and either $\gamma = 1$ or $\gamma = 1.2$. It is required to have E_{gas} as given by equation 6, using $K = 1.2$ for Models A and B, and $K = 1.5$ for Models C and D. Default profiles have roughly the values of η_{200} shown (which is a function of the concentration c). The above E_{gas} is then increased by adding any excess specific energy. The heated profile is found by searching along lines of constant η_{200} or γ , depending on the heating model as shown. Models A and C have to take into account the upper limit of $\gamma = 5/3$.

fitted by the $\gamma = 1$ profiles than by $\gamma = 1.2$ profiles (Ettori, private communication). Hence we have chosen to calibrate K in this case only by matching to the $L_X - T$ relation measured by Allen & Fabian (1998a). As above, we require the gas fractions of all model clusters to be equal to 0.17. We find that $K = 1.5$ results in an $L_X - T$ distribution which best fits the data. The resulting clusters have $\eta_{200} \approx 28$. An example of such a gas halo is shown in Figs 2 to 4 as dot-dashed curves, for comparison with the solid curves ($\gamma = 1$ and $\eta_{200} = 10$). Notice that although the two density profiles have different shapes, they roughly follow each other, intersecting at two points. The higher value of $\eta_{200} = 28$ merely implies that the temperature at r_{200} is lower by a factor of 2.8 compared to the $\eta_{200} = 10$ case (Fig. 3).

In both types of default profile, since γ is fixed, it is not hard to show that η is a function of the NFW concentration c only. As shown in Fig. 1, the largest clusters have a small scatter in c (Fig. 1), hence their scatter in η is also small. This is why, in the absence of excess energy, the model clusters are very close to being self-similar (see also WFN98), even though they are not exactly self-similar due to the variation in c .

Having described how to obtain a default gas profile, we now need to specify how the gas profile changes due to heating. We shall model this in two ways: by decreasing η_{200} while keeping γ constant, or by increasing γ while keeping η_{200} constant. The former has the effect of increasing the temperature at all radii by the same amount (to see this, multiply equation 11 by T_{200} and note that $\eta_{200}T_{200}$ remains constant). The latter steepens the temperature gradient while ensuring that the temperature at r_{200} stays constant, so that heating is concentrated towards the centre.

Since there are two types of default profile, we have four heating models in total. These are summarized in Fig. 5. Models A and B have default profiles with $\gamma = 1$ and Models C and D have default profiles with $\gamma = 1.2$. Heating increases γ in Models A and C, but decreases η_{200} in Models B and D. Notice that for Models B and D, it is not necessary to know the default profile in order to

find the heated profile. Hence the heated profile can be obtained in one stage rather than two.

There are a few loose ends to tie up. If the excess energy is so high that the total energy of the gas is positive, then the gas is not bound and it does not form a halo. However, for Models A and C, one may need to search ‘beyond’ $\gamma = 5/3$ for halos which have very high excess energies but are still bound. In this situation one searches in the $-\eta_{200}$ direction while keeping $\gamma = 5/3$ (see Fig. 5).

5 SETTING THE MODEL PARAMETERS

To summarize, there are 3 parameters related to the gas processes that need to be set. They are the critical ratio of cooling time to free-fall time, τ_0 , the efficiency of supernova feedback, ϵ_{SN} , and the boost in the rate of supernovae. As discussed in section 2.3, we boost supernova rates by a factor of 5 in this paper. We keep the other two parameters constant for each heating model (hence each simulation), but they are allowed to differ between heating models.

We consider Models A and B only in this and the following section. In section 7 we shall use all four heating models to simulate clusters, but not galaxies. In those simulations, the precise values of τ_0 and ϵ_{SN} are not required. This is because the collapses only produce hot gas given any reasonable value of τ_0 . As a result, no stars form and ϵ_{SN} is not required.

The cosmological parameters used in this paper are given in section 1, which imply an initial gas fraction of 0.27. We note that the resulting model clusters (section 6) have gas fractions of 0.17 (with a scatter of about 0.01), which therefore match the average cluster gas fraction measured by Evrard (1997) and Ettori & Fabian (1999), assuming $h = 0.5$.

5.1 Setting ϵ_{SN}

The feedback parameter ϵ_{SN} controls the amount of star formation, which can be characterized by the fraction of gas turned into stars by the present day. Using the Coma cluster as a large sample of baryons, the mass ratio of hot gas to stars inside a radius of $1.5h^{-1}$ Mpc is about 15, using $h = 0.5$ (White et al. 1993). In order to match this, we set $\epsilon_{\text{SN}}=0.3$ for Model A and $\epsilon_{\text{SN}}=0.25$ for Model B. We find that the required value of ϵ_{SN} is almost independent of the value of τ_0 , unless τ_0 takes an ‘extreme’ value (see below). We note from the initial and cluster gas fractions given above, that a much larger fraction of baryons is turned into BDM than into stars. The bulk of the BDM is formed in the halos of large galaxies and small groups.

5.2 Setting τ_0

The parameter τ_0 controls the transition from cold to hot collapse. In addition, increasing τ_0 results in the galaxies of larger halos becoming classified as dwarf galaxies, when they would previously be counted as normal galaxies (this is because a larger τ_0 reduces the amount of BDM that forms in a given halo). The remaining normal galaxies then belong to more massive halos which thus have longer cooling times. As a result, they are less likely to cool out all of their hot gas and form spiral galaxies.

In other words, increasing τ_0 also increases the elliptical fraction of normal galaxies. We calibrate τ_0 by requiring the elliptical fraction in the field (i.e. among normal galaxies that do not occur in groups) at the present time to be 0.1, which is roughly the value obtained by Postman & Geller (1984) in their least dense regions.

Table 1. Values of ϵ_{SN} and τ_0 used in section 6. See text for a full discussion.

	ϵ_{SN}	τ_0
Model A	0.3	1.0
Model B	0.25	0.4 (gives incorrect elliptical fraction)
Model B	0.15	0.1

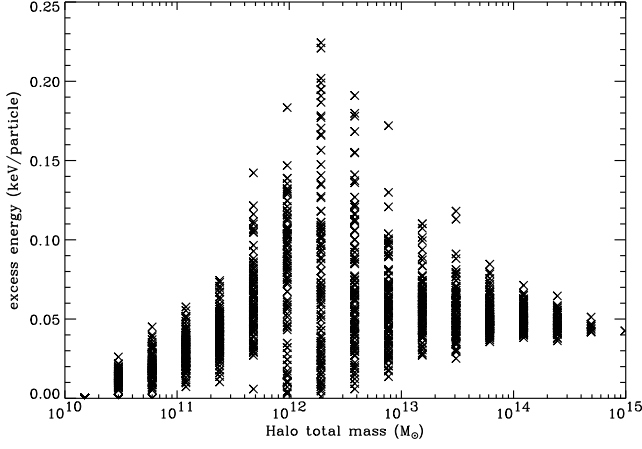


Figure 6. Scatter plot of excess energy vs. halo mass, using Model A. Each mass contains a maximum of 100 points. Halos were selected randomly from the simulation regardless of redshift.

For Model A we are able to fit this using $\tau_0 = 1$. However, for Model B we find that we require a much lower value of τ_0 . Even with $\tau_0 = 0.4$, Model B gives a high elliptical fraction of 0.65 in the field. The constraint is satisfied using $\tau_0 = 0.1$, but this is so low that it increases the cluster gas-to-stellar mass ratio to 38 (due to a lack of star formation). We are able to satisfy both constraints using $\tau_0 = 0.1$ if we lower ϵ_{SN} to 0.15.

This appears to be a fundamental problem with Model B (in our chosen cosmology). In both Models A and B, the gas halos of normal galaxies have substantial excess energies due to the supernovae of progenitor halos (section 6). However, heating increases temperature uniformly in Model B, whereas the temperature at r_{200} hardly increases in Model A. Hence, in Model B the cooling time at r_{200} is increased substantially by excess energy (the cooling function is very steep around 10^6 K), which makes it harder for all the gas to cool and form a disk. This is why the elliptical fraction is much higher in Model B.

The results for ϵ_{SN} and τ_0 are displayed in Table 1.

6 RESULTS FROM THE COMPLETE SIMULATIONS

Complete galaxy and cluster simulations were carried out with Models A and B, using the parameters in Table 1. For each simulation we used 100 realisations of the merger tree.

6.1 Excess energies from supernova heating

For Model A, we display a scatter plot of excess energies vs. total halo mass in Fig. 6. All of the plots in this section were generated by selecting randomly up to 100 halos for each mass, regardless of redshift. Only the most massive halos have less than 100 points

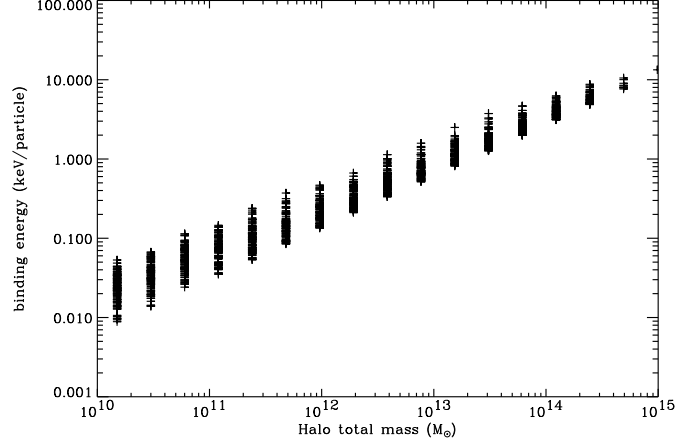


Figure 7. As Fig. 6, but showing the magnitude of the binding energy vs. halo mass. Note that the energy is now plotted logarithmically.

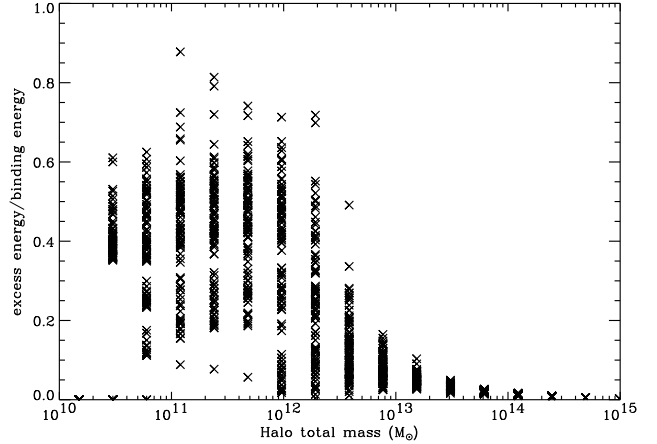


Figure 8. As Fig. 6, but showing the ratio of excess energy to binding energy.

plotted, because they are so scarce. We measure specific energies in terms of the energy per μm_{H} of gas mass, where the gas is assumed to be fully ionized, and express the result in units of keV/particle.

The excess energies in Fig. 6 tend to increase with mass up to $\sim 10^{12} M_{\odot}$, when star formation gives way to cooling flow behaviour. For more massive halos, the mean excess energy changes little, but the scatter reduces significantly due to an averaging effect. However, a gradual decrease can be detected in the most massive halos, due to dilution by the accretion of primordial gas.

To obtain a more physically informative plot, we calculate the ratios of excess energy to binding energy. This gives a measure of the excess energy's ability to change the gas distribution. Recall that we define binding energy to be the value of $|E_{\text{gas}}|$ in the absence of excess energy. Fig. 7 shows a scatter plot of binding energy vs. halo mass for the same simulation using Model A. The scatter plot of the resulting ratios of excess energy to binding energy is displayed in Fig. 8. The ratio has an upper limit of 1, above which gas halos are not bound. For halos smaller than $\sim 10^{12} M_{\odot}$, the points are distributed between 0.2–0.6, fairly independently of halo mass.

This result can be understood as follows. Below a certain halo mass, almost all of the galaxies produce sufficient supernova en-

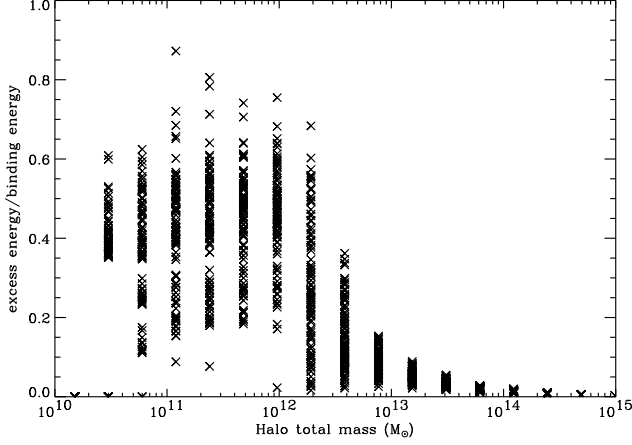


Figure 9. The ratio of excess energy to binding energy obtained from Model B, using $\tau_0 = 0.4$ and $\epsilon_{\text{SN}}=0.25$. Note the strong similarity with Fig. 8.

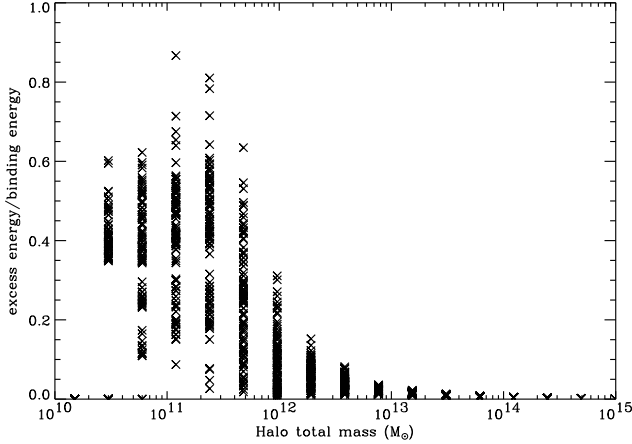


Figure 10. The ratio of excess energy to binding energy obtained from Model B, using $\tau_0 = 0.1$ and $\epsilon_{\text{SN}}=0.15$. The lower value of τ_0 causes star formation to cease at lower masses, resulting in a notable difference from Fig. 9.

ergy to eject their gas. In addition, the excess energy of gas that is ejected is always equal to the binding energy of the halo it belonged to (because the model assumes that gas is ejected at the escape velocity). Thus for a halo in the above mass range, or even a few times more massive, its ratio of excess energy to binding energy simply reflects the ratio of the binding energies of its progenitors to itself. (To be precise, we should also take into account the primordial gas accreted, which contributes no excess energy of its own.) The fact that the distribution shown in Fig. 8 is a weak function of mass below $\sim 10^{12} M_{\odot}$ means that the said ratios do not change much with mass scale. However, for halos more massive than $\sim 10^{12} M_{\odot}$ the ratio drops dramatically, due to a cessation of star formation. In particular, the ratios are so small in halos more massive than $10^{14} M_{\odot}$ that the excess energies must have hardly any effect on the gas profiles of clusters.

Since the behaviour observed in Fig. 8 can be attributed to the binding energies of halos, it should depend little on the heating model. For comparison, we show the corresponding plot for Model

B in Fig. 9, using the parameters $\tau_0 = 0.4$ and $\epsilon_{\text{SN}}=0.25$. It is almost the same as for Model A.

However, a difference does occur if we use a much lower value of τ_0 . We illustrate the effect in Fig. 10, where we have used the parameters $\tau_0 = 0.1$ and $\epsilon_{\text{SN}}=0.15$ with Model B (as given in Table 1). In this case the lower value of τ_0 restricts star formation to smaller halos, so that the ratio of excess energy to binding energy drops off at a lower mass scale. Note that this scenario should not occur in reality, not only because we expect $\tau_0 \sim 1$, but because the resulting luminosity function, after fitting with a Schechter function, would yield a value for L_* that is too small.

6.2 Excess energy and iron abundance of clusters

We find that the excess specific energies of clusters are *not sensitive* to ϵ_{SN} and the number of supernovae per unit star formation. For example, using $\epsilon_{\text{SN}}=0.1$ and 1.0 with Model A give virtually identical cluster excess energies to those shown in Fig. 6—indeed, the rest of the plot is hardly modified. Changing instead the boost in supernova rates from 5 to 1 only reduces cluster excess energies from around 0.05 to 0.03 keV/particle.

The reason for these perhaps surprising results is as follows. Consider moving backwards in time along a merger tree, into all the ‘branches’ emanating from a cluster, and stopping at the last halos that produced (type II) supernovae in each of these branches. It is not hard to see that the excess specific energy of the cluster is largely determined by the excess energies resulting from these last halos—dilution by primordial gas does occur in later collapses, but the extent of this is mostly determined by the merger tree. For those ‘last halos’ that ejected their atmospheres, the gas ejected from them were given excess specific energy equal to the binding energy of the halo; those halos that did not eject their atmospheres (because they contained sufficient hot gas) left their gas with less excess specific energy, but more than what the hot gas had to begin with, which is in general a substantial fraction of the binding energy (see halos of order $10^{12} M_{\odot}$ in Fig. 8). In conclusion, the excess specific energies of clusters are roughly determined by the *binding* energies of these ‘last halos’, which is why we do not expect them to be sensitive to the efficiency of supernova heating.

So what caused the reduction in cluster excess energies in the example above? By reducing supernova rates by a factor of 5, the amount of star formation in the smallest galaxies increased by the same factor, consuming 5 times more gas. As a result, the gas fraction in the so-called ‘last halos’ were much lower. This implied longer cooling times and less (possibly no) cold gas. Hence the excess specific energy resulting from such halos was reduced.

The above suggests that the excess energies of clusters can be raised by increasing τ_0 (if we ignore the effect of this on other properties). By increasing τ_0 to 3, we found that the transition to hot collapse was shifted to halos that were roughly 4 times more massive. As a result, the excess energies of clusters increased from around 0.05 to 0.12 keV/particle. The binding energies of halos roughly scale as mass to the power of 2/3, thus it is interesting that the excess energy has scaled roughly as the binding energy of the ‘last halos’, for $0.12 \approx 4^{2/3} \times 0.05$. Note that the amount of freedom in τ_0 is limited, as it determines the position of the exponential drop-off in galaxy luminosity functions. In some SAMs that do not include cooling flows, star formation is turned off in halos with circular velocities $\gtrsim 400$ km/s (Somerville & Primack 1998).

Taking a different approach, it is useful to consider what happens to the energy injected by supernovae. Using the gas-to-stellar mass ratio of 15 that we required in clusters ($> 10^{14} M_{\odot}$), we can

easily estimate the excess specific energy if all of the supernova energy associated with the stars is retained in the intra-cluster gas. As used in Model A, we assume $4 \times 10^{50} \epsilon_{\text{SN}}$ erg per supernova where $\epsilon_{\text{SN}}=0.3$. The excess energy thus obtained is 0.16 keV/particle. This is about 3 times higher than in Fig. 6. However, it does not account for the energy injected into gas that later formed BDM: roughly 10/27 of all baryons. Accounting for this gives $0.16 \times 17/27 = 0.1$ keV/particle. In addition, we found that roughly *half* of this is radiated away in cold collapses. This brings the excess energy down to about 0.05 keV/particle, as shown in Fig. 6. We note that even if we remove the ‘correction’ due to BDM given above, the excess energy in clusters would still be only $0.16/2 = 0.08$ keV/particle.

The amount of excess energy lost in cold collapses was deduced by comparing the excess specific energy of a cluster to the value expected from the iron abundance of the gas. In the absence of radiative cooling, the two values would be the same in the simulations (because they come from the same supernovae). However, the excess specific energy is reduced if the gas radiates its thermal energy, but does not turn into stars or BDM. This is what happens to most of the gas in cold collapses. We found the excess specific energy of clusters to be always roughly half the value expected from the iron abundance. This highlights the uncertainty of estimating excess specific energy from iron abundance. The energy lost in this way is in addition to the energy radiated immediately after supernova explosions (which we account for using ϵ_{SN}).

The iron abundance of the clusters shown in Figs. 8 and 9 are about $0.08 Z_{\odot}$, which is lower than the observed range of 0.2– $0.3 Z_{\odot}$ (Fukazawa et al. 1998). We reiterate that this is not the reason for their low excess energies. Indeed, since the bulk of star formation in our model occurs in massive bursts that result in gas ejection, it is more appropriate to say that the binding energy of these galaxies determine the amount of star formation and metal enrichment that occurs. Thus, we find that reducing ϵ_{SN} by a factor of 3 increases the stellar mass and iron abundance of clusters by about a factor of 3. Although we required the gas-to-stellar mass ratio of clusters to be 15 (White et al. 1993), due to the uncertainty in the mass-to-light ratio of cluster galaxies, a lower value of 5 is also possible. We note that a large fraction of iron is injected into gas that later forms BDM, as was the case with excess energy.

The large number of type II supernovae per unit stellar mass required to enrich cluster gas to observed metallicities has been discussed by other authors (Arnaud et al. 1992; Elbaz, Arnaud, & Vangioni-Flam 1995; Brighenti & Mathews 1998). It is possible that a large fraction of the iron in cluster gas is due to type Ia supernovae, which we have not included. Nagataki & Sato (1998) suggest that between 30–90 per cent of the iron in clusters may be due to type Ia supernovae. It is also possible that the observed metallicities (which are emission-weighted) overestimate the average metallicities of cluster gas, as a result of steep metallicity gradients (Ezawa et al. 1997; Allen & Fabian 1998b).

6.3 The effect on galaxy formation

What is the effect of the high excess energy-to-binding energy ratios on star formation in galaxies?

We investigated this question using Model A by considering what happens if default gas profiles are used in all halos, regardless of excess energy. By comparing the results from our fiducial model to the results when only default profiles were used, we were able to see the difference made by supernova heating.

Fig. 11 shows a scatter plot of the fraction of gas in a halo that formed stars as a function of halo mass. As explained in section 2.3,

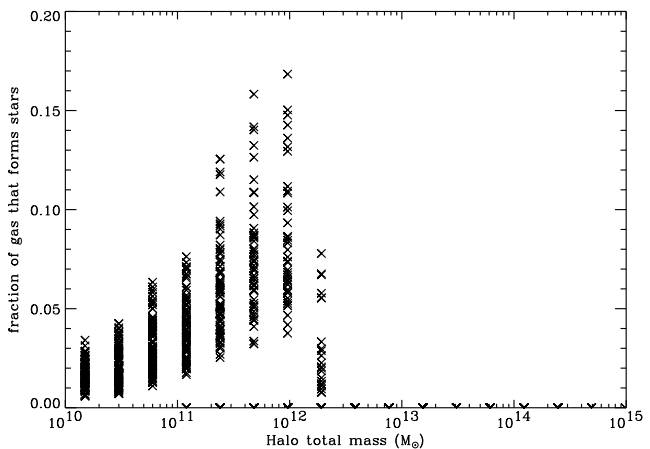


Figure 11. Scatter plot of the fraction of gas in the halo that formed stars, using Model A. As explained in section 2.3, this is the mass of stars formed with $M < 1M_{\odot}$.

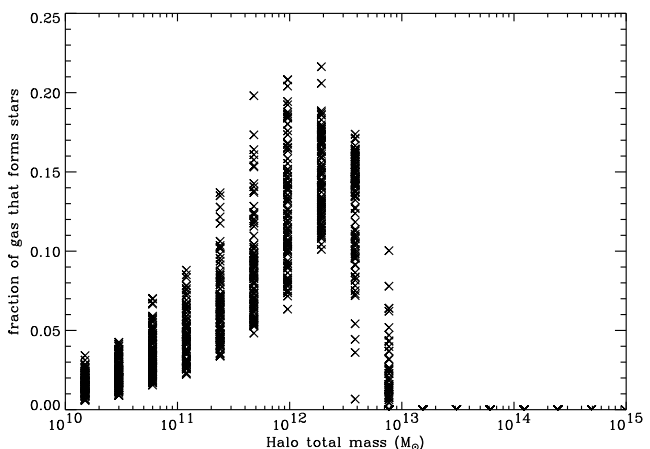


Figure 12. As Fig. 11, except that default gas profiles were used in all halos, regardless of excess energy. A dramatic increase in star formation occurs in halos in the mass range 10^{12} – $10^{13}M_{\odot}$.

this is the mass of stars formed with $M < 1M_{\odot}$. The data are taken from the same halos shown in Figs. 6 to 8. From a separate simulation, Fig. 12 shows the same when only default gas profiles were used. No other factors in the model were changed. Fig. 12 shows a dramatic increase in the amount of star formation for halos in the mass range 10^{12} – $10^{13}M_{\odot}$, which become some of the most efficient star-forming galaxies. These halos experienced little star formation in our fiducial model because most if not all of their gas was hot after virialization.

Excess energy from supernovae thus regulates the transition from cold to hot collapse as we move up in mass scale. By increasing cooling times and making hot collapses more likely, excess energy moves the onset of hot collapse to smaller mass scales. This effect is model-independent.

Some SAMs turn off star formation and/or cooling in halos with circular velocities greater than ~ 400 km/s (Somerville & Primack 1998), so as not to produce an excess of superluminous galaxies. Our results suggest that this problem could be solved by

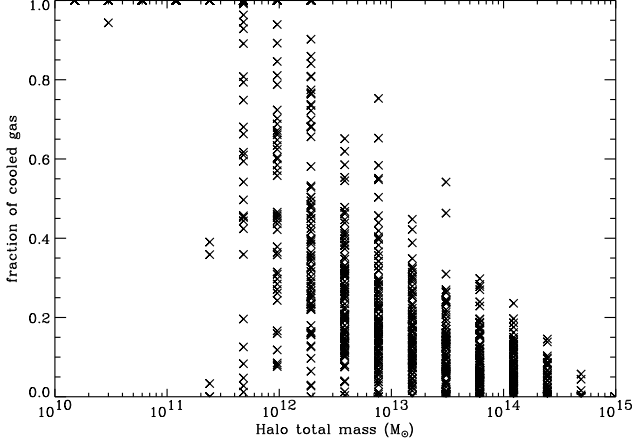


Figure 13. Scatter plot of the fraction of gas with cooling time shorter than the time to the next collapse, for Model A. The apparent lack of points for low mass halos is because they all have the same value at the top of the plot.

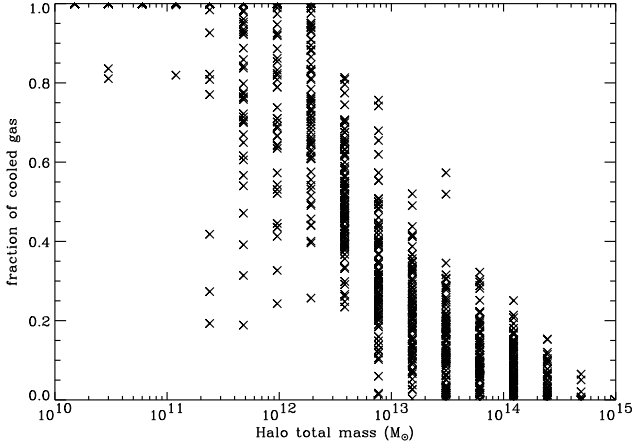


Figure 14. As Fig. 13, except that default gas profiles were used in all halos. The main difference with Fig. 13 occurs in the mass range 10^{12} – $10^{13} M_{\odot}$.

modelling cooling flow behaviour in hot gas and regulating this with excess energy from supernovae.

In our model, ignoring the effect of excess energy on gas profiles has additional important consequences. Halos of $\sim 10^{12} M_{\odot}$, whose galaxies are classified as normal galaxies in our fiducial model, become dominated by cold instead of hot gas. As a result, they form enough stars to eject their atmospheres and become classified as dwarf galaxies.

It is interesting to note that there is little change between Figs. 11 and 12 for halos below $5 \times 10^{12} M_{\odot}$. Most, if not all of the gas in these halos undergo cold collapse. Hence excess energy from supernova heating makes little difference to the results, as one might expect.

Since different SAMs handle cooled gas differently, it is useful to consider a more model-independent quantity. Figs. 13 and 14 show the same halos used in Figs. 11 and 12, respectively, but we now plot the fraction of gas whose cooling time is shorter than the time to the next collapse (i.e. major merger). Once again, the most difference is observed in halos of mass 10^{12} – $10^{13} M_{\odot}$, where the fractions in Fig. 14 are roughly double those in Fig. 13. For these

Table 2. Best fitting values of excess energy for each heating model, obtained by matching to the $L_X - T$ relation measured by David et al. (1993). Excess energy per particle is calculated as $(\mu m_H \Delta E_{\text{gas}})$.

Heating Model	Excess Energy (keV/particle)
A	1.8
B	2.8
C	2.2
D	3.0

halos, we therefore expect the amount of star formation in general to be strongly influenced by excess energy from supernovae. For more massive halos, the excess specific energies become too small to have significant effect on the gas profiles.

7 THE EXCESS ENERGIES REQUIRED IN X-RAY CLUSTERS

In WFN98 we were able to fit the properties of X-ray clusters with a model that used isothermal profiles only (Model B in this paper). The data we reproduced included the $L_X - T$ relation, the temperature function, the luminosity function and the mass deposition rate (\dot{M}) function. An essential ingredient was the inclusion of excess energy, at the level of about 1 keV/particle. This was needed to break the self-similarity of clusters with $L_X < 2 \times 10^{45} \text{ erg s}^{-1}$, which would otherwise follow the scaling relation $L_X \propto T^2$ instead of the observed relation $L_X \propto T^3$.

Here we present the results for clusters obtained using each of the four heating models. The simulations are ‘low resolution’ in the sense that they only use the top 10 levels of the collapse tree simulated in the previous section. Hence, the smallest regions have masses of $1.5 \times 10^{13} M_{\odot}$. Each simulation used a total of 10000 realisations of the merger tree. Unlike the previous section, where the amount of gas in a cluster depended naturally on the amount used up by star formation and cooling flows, we have set the gas fraction of every cluster to be 0.17 (Evrard 1997; Etti & Fabian 1999) for definiteness. This is slightly higher than the average value of 0.14 obtained in WFN98. The formulae used to calculate bolometric luminosity L_X , emission-weighted temperature T and the mass deposition rate of cooling flows are given in Appendix A. All quantities have been evaluated at $z = 0$. We have improved the estimation of mass deposition rates by calculating an instantaneous rate instead of an average rate over the lifetime of a cluster (WFN98). In each simulation we gave all the clusters a constant excess specific energy. For each heating model, we then found the excess energy required in order to fit the observed data.

The required excess energies were found by matching to the $L_X - T$ relation of David et al. (1993). In Table 2 we give the best-fitting excess energy for each heating model. The resulting $L_X - T$ distributions are displayed in Figs 15 to 18. The scatter in the distributions arise naturally from our model. When compared to the excess energies used in WFN98, the excess energies in Table 2 are somewhat higher. This is partly due to the higher gas fraction used here and partly due to the better fits obtained in Figs. 15 to 18, especially for clusters with temperatures of 3–4 keV. The slopes of the distributions given by Models B and D are slightly steeper than the observed slope. This suggests that we need to relax our assumption of constant excess energy for all clusters.

As expected, Models A and C require less heating than the other models, because they concentrate heating towards the centre of clusters, where most of the luminosity comes from. In addition,

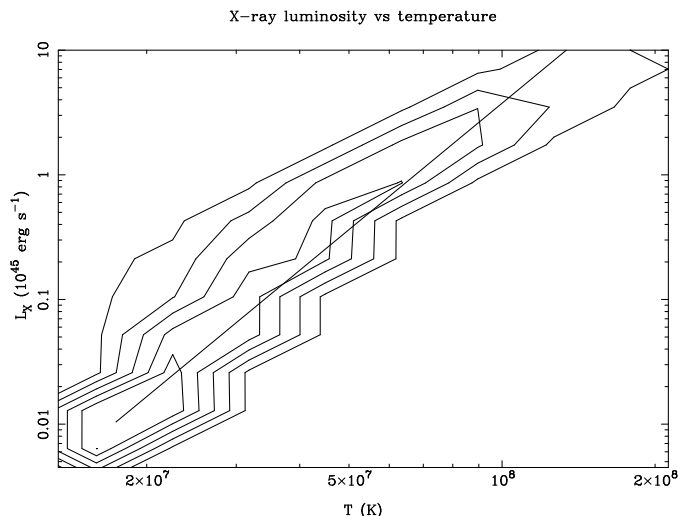


Figure 15. Contour plot of the cluster X-ray luminosity-temperature distribution obtained for Model A, with heating included at the level given in Table 2. The contours are spaced at equal logarithmic intervals. The long straight line is the best fit (for bolometric luminosities) taken from David et al. (1993). The extent of the line corresponds roughly to the extent of the data.

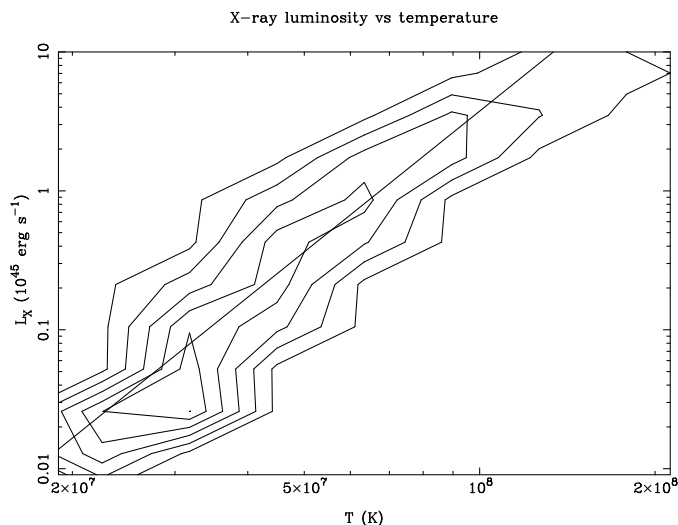


Figure 16. Same as Fig. 15 but using Model B.

Models C and D require slightly more excess energy than Models A and B. However, the largest excess energy in Table 2 is only about 50 per cent higher than the smallest, over a set of very different heating models.

We display the X-ray luminosity function, temperature function and mass deposition rate (\dot{M}) function from the above simulations in Figs. 19, 20 and 21, respectively. In each plot we have used a different line for each heating model. Superimposed on each plot is the observed data, as described in the captions. Note that for the \dot{M} function we have not included model clusters cooler than 2×10^7 K. This is because the data used for comparison (Peres et al. 1998) was obtained from the brightest 55 clusters in the sky in the 2–10 keV band. Hence clusters which are too cool were not included in the sample.

The luminosity and temperature functions obtained with all

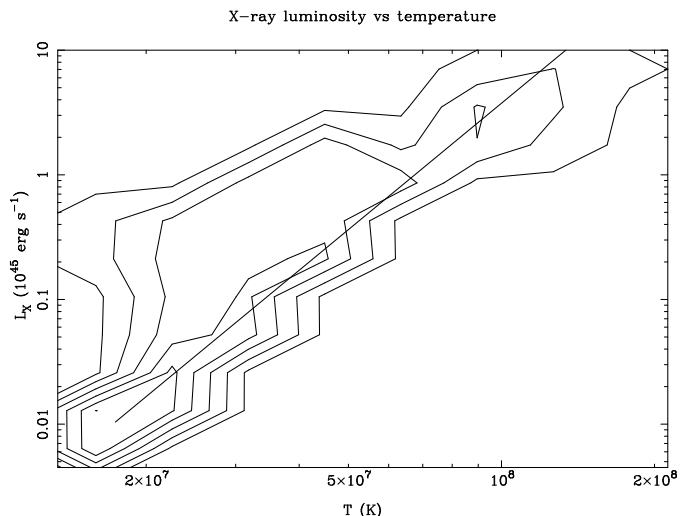


Figure 17. Same as Fig. 15 but using Model C.

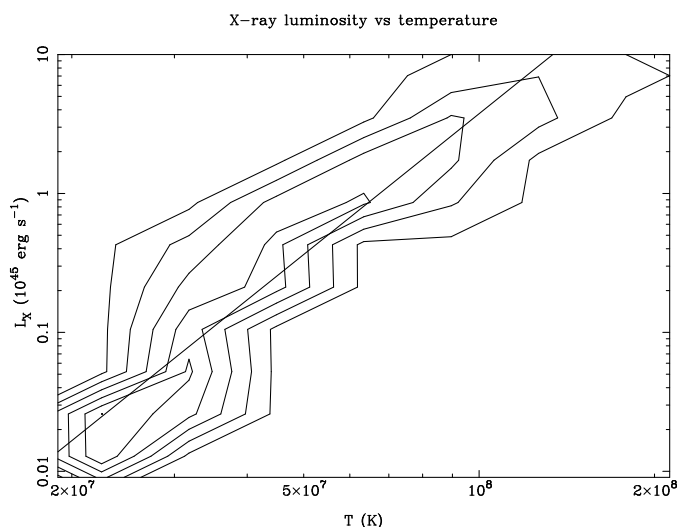


Figure 18. Same as Fig. 15 but using Model D.

four heating models give good fits to the data. However, the model \dot{M} functions give relatively poor fits to the data.

Models C and D give particularly poor fits where $\dot{M} > 100 M_\odot \text{ y}^{-1}$. This is because the mass deposition rate of large clusters are too high in these models. This can be attributed to the flatter cores of their gas density profiles. The poor performance of Models C and D support the result that profiles with $\gamma = 1.2$ do not fit the surface brightness profiles of large clusters as well as profiles with $\gamma = 1$ (Ettori, private communication).

Models A and B show a deficit of clusters with small cooling flows ($\dot{M} = 10\text{--}100 M_\odot \text{ y}^{-1}$). This is in contrast to our result in WFN98, where we obtained a good fit to the \dot{M} function using Model B. The main reason for this difference is because the excess energies are now much higher. In particular, they are too high for the smallest clusters. We repeated the simulation for Model B using lower excess energies in clusters less massive than $246 \times 10^{12} M_\odot$. Table 3 gives the excess energies that we used, which increase steadily with mass up to $246 \times 10^{12} M_\odot$. The resulting $L_X - T$ distribution and \dot{M} function are shown in Figs. 22 and 23.

The $L_X - T$ distribution shown in Fig. 22 gives a better fit

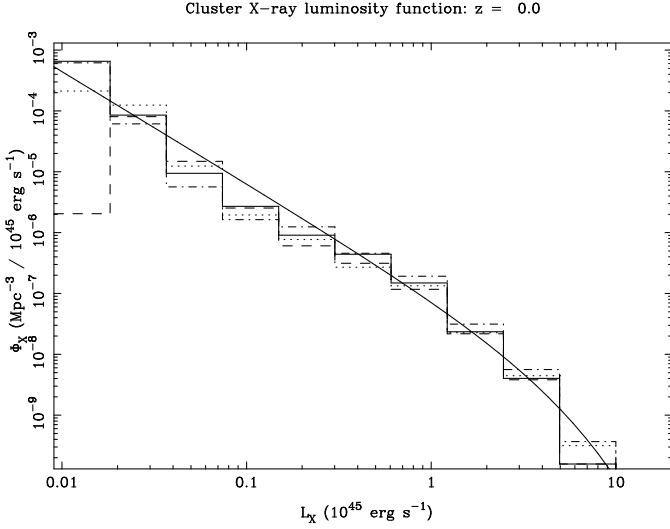


Figure 19. The X-ray luminosity functions for all four heating models. The model results are plotted as follows: Model A: solid line, Model B: dashed line, Model C: dot-dashed line, Model D: dotted line. The curve is the best-fitting Schechter function for the *ROSAT* Brightest Cluster Sample bolometric luminosity function (Ebeling et al. 1997).

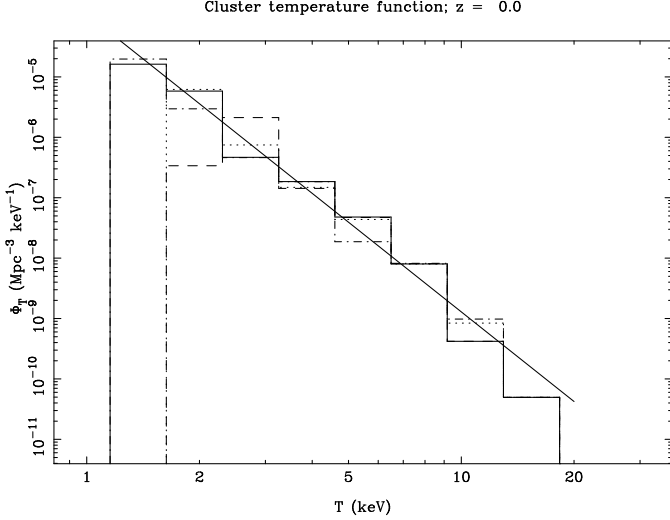


Figure 20. The X-ray temperature functions for all four heating models, plotted with the same line styles as in Fig. 19. The straight line is the power law fit obtained by Edge et al. (1990).

Table 3. The set of excess energies used with Model B to improve the \dot{M} function, as shown in Fig. 23.

Halo Mass ($10^{12} M_{\odot}$)	Excess Energy (keV/particle)
≥ 246	2.8
123	2.3
61	1.9
35	1.5
15	1.1

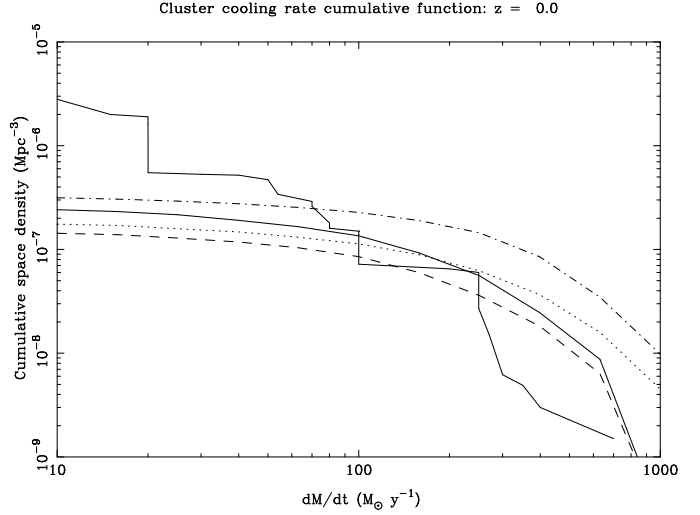


Figure 21. The mass deposition rate functions (plotted cumulatively) for all four heating models, plotted with the same line styles as in Fig. 19. The jagged line is the same function taken from Peres et al. (1997), modified by using a cluster age of 6 Gyr. We also exclude model clusters cooler than 2×10^7 K from this plot, as they would not be included in the sample used by Peres et al..

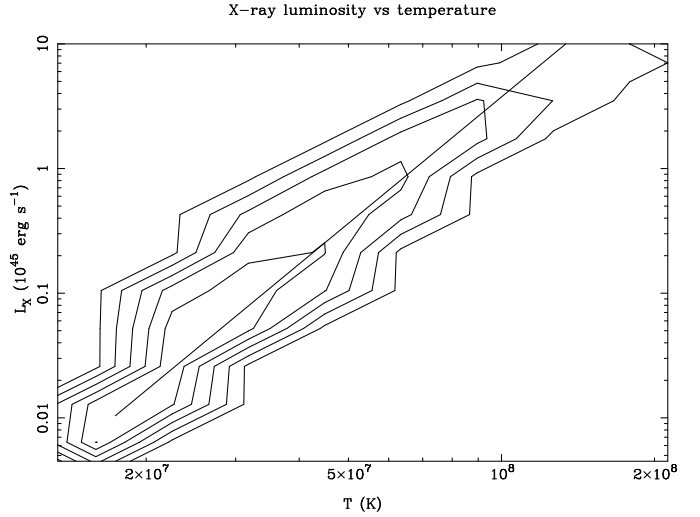


Figure 22. As Fig. 16, but using increasing excess energies with halo mass, as given in Table 3. Model B was used. Previously unbound groups now appear at temperatures below 2 keV.

to the data than that shown in Fig. 16. The new distribution also reaches to lower temperatures. This is because a large number of clusters with temperatures of around 2×10^7 K were unbound by the high excess energy used before. Hence these clusters did not appear in Fig. 16. The \dot{M} function shown in Fig. 23 also matches the data much better than before, due to the increased number of clusters with small cooling flows.

If it is true that excess specific energies increase with cluster mass, then this represents a considerable difficulty for heating by supernovae. This is because we expect the excess specific energy to become more diluted in larger clusters (section 6). However, a possible way around this problem is to combine different heating models. If large clusters are preferentially heated towards the centre (as in Model A) but small clusters are heated more uniformly (as in

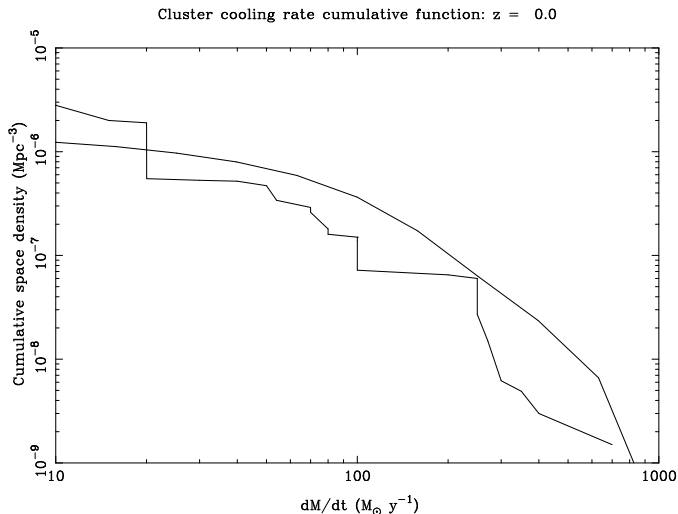


Figure 23. As Fig. 21 but for Model B only, using increasing excess energies with halo mass as given in Table 3. The number of small cooling flows has increased, improving the fit to the data.

Model B), then it is possible that an excess energy of roughly 1.8 keV/particle across all clusters could satisfy all the data (see Table 2 and 3). Such a scenario may arise as a result of a characteristic scale in the distribution of the heat source (supernovae or AGN), or in the redistribution of heated gas. The latter is made plausible by the fact that the excess energies are close to the binding energies of the smallest clusters, but are smaller than the binding energies of larger clusters.

7.1 Using all available gas profiles

Even the lowest excess energies required above are higher, by over an order of magnitude, than those obtained from supernova heating in our complete simulations (section 6). By using all the available gas profiles (i.e. independently of any heating model), we have also found the minimum excess energy required to put a fiducial cluster on the observed $L_X - T$ relation.

We considered the specific case of a halo of mass $1.23 \times 10^{14} M_\odot$, with a virialization redshift of $z = 0$ and a gas fraction of 0.17 (as before). Such a cluster has a temperature of around 2 keV, depending on the amount of heating. To obtain the NFW profile we assumed the same cosmology as before. We structured the problem as follows. First, we found the locus of points in (η_{200}, γ) -space which put the cluster on the observed $L_X - T$ relation. From these points we then found the one which had the least excess energy. However, the gas profile specified by (η_{200}, γ) only tells us the value of E_{gas} —the excess energy depends on the value of E_{gas} in the absence of non-gravitational heating. In what follows, we shall use equation 6 and $K = 1.2$ to obtain the ‘default’ value of E_{gas} (as in Models A and B). This implies that the default gas profile is isothermal, but we shall also consider other possibilities.

Fig. 24 shows contours of constant excess energy, labelled in keV/particle. The gas halo becomes unbound for excess energies above 3.1 keV/particle. The dashed curves are contours of constant $T/L_X^{0.297}$, where T is emission-weighted temperature in keV, and L_X is bolometric luminosity in units of $10^{40} \text{ erg s}^{-1}$. The units are the same as in David et al. (1993), who obtained the best-fitting power law $T/L_X^{0.297} = 0.19$. The contour labelled 0.19 therefore gives the set of parameters which result in clusters with observed

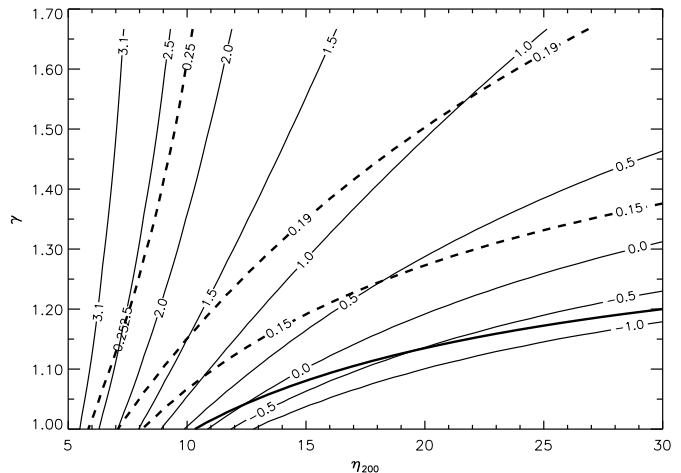


Figure 24. Contour plot in parameter space for a fiducial cluster of mass $1.23 \times 10^{14} M_\odot$, collapsing at $z = 0$ with a gas fraction of 0.17. The three dashed contours follow points of constant $T/L_X^{0.297}$ (see text); the middle one results in clusters which lie on the observed $L_X - T$ relation (David et al. 1993). The thin contours are labelled by excess energy (keV/particle), measured relative to a $\gamma = 1$ default profile (as in Models A and B). The thick solid line roughly sweeps out the locations of other possible default profiles. The profile that requires the least excess energy to match the $L_X - T$ relation is given by $\gamma = 5/3$ and $\eta_{200} = 27$. It has an excess energy of 0.9 keV/particle. (See text for full discussion.)

properties. Two other dashed contours are shown, corresponding to $T/L_X^{0.297} = 0.15$ and 0.25. From the plot, the gas profile with $\gamma = 5/3$, $\eta_{200} = 27$ requires the least excess energy to match the observed data. This profile has an excess energy of 0.9 keV/particle. That this cluster is marginally stable to convection ($\gamma = 5/3$) should not be surprising. We ‘save energy’ by concentrating the heating where it makes the most difference, i.e. near the centre, but convection limits the extent to which we can do this. The gas halo that requires the least heating is therefore the one whose atmosphere is marginally stable to convection. This suggests that the $\gamma = 5/3$ profile probably requires the least heating among all possible gas profiles.

Is it likely that the excess energy is this low in reality? To answer this, we considered whether the $\gamma = 5/3$ gas profile would be a viable candidate for a typical cluster at the same temperature of 1.6 keV. Fig. 25 shows the temperature and entropy of all the gas profiles. The entropies have been calculated at a radius of $0.1r_{200}$, for comparison with observed entropies at the same radii (Ponman et al. 1999). The $\gamma = 5/3$ profile has an entropy of $T/n_e^{2/3} = 600 \text{ keV cm}^2$, which is roughly 3 times larger than the entropies observed in clusters of a similar temperature (we have assumed $h = 0.5$ in the results of Ponman et al.). The $\gamma = 1$ profile that satisfies the $L_X - T$ relation gives an entropy of 220 keV cm^2 , which agrees with the observed entropies. We note that the model entropies are slightly biased towards higher values because of the virialization redshift of $z = 0$, but it is clear that the observations strongly favour γ close to 1. We have studied the same cluster virializing at a redshift $z = 0.5$ and the conclusions remain the same.

So far we have assumed that in the absence of heating $E_{\text{gas}} = -3.1 \text{ keV/particle}$, as given by equation 6 using $K = 1.2$. If we use $K = 1.5$ instead (as in Models C and D), then the default value of E_{gas} becomes $1.5/1.2 \times (-3.1) \approx -3.9 \text{ keV/particle}$. As this is lower than before, all excess energies are *increased* by

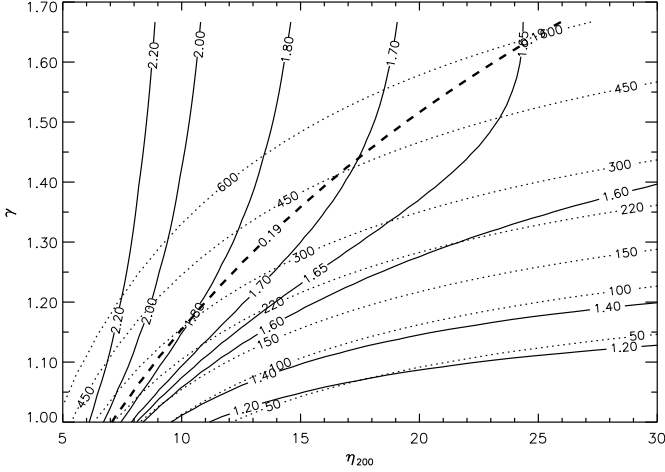


Figure 25. Thick dashed line as in Fig. 24. This plot shows contours of emission-weighted temperature (solid lines), and entropy at a radius of $0.1r_{200}$ (dotted lines), following Ponman et al. (1999). The former are labelled in keV, the latter in keV cm^2 .

0.8 keV/particle. We can generalize further by considering what parameters the cluster would need in order to lie on the self-similar relation $L_X \propto T^2$ normalized to the largest observed clusters. The assumption is that in the absence of non-gravitational heating or cooling all clusters would follow this relation, whereas in reality it is followed asymptotically by the largest clusters only. We normalize the relation to pass through $T = 10^8 \text{ K}$ and $L_X = 4 \times 10^{45} \text{ erg s}^{-1}$, roughly following the results of Allen & Fabian (1998a). The gas profiles which satisfy this relation are given by the thick line in Fig. 24. As expected, it passes close to the points $(\eta_{200}, \gamma) = (10, 1)$ and $(28, 1.2)$, where the default profiles of our heating models are found. Thus the thick line roughly sweeps out the locations of possible default profiles. It is clear that using a $\gamma = 1$ default profile, as we assumed to begin with, gives the highest default value of E_{gas} . Hence the excess energies given in the plot are also the lowest possible values.

In conclusion, our results suggest that the absolute minimum excess energy in a cluster of this mass is about 0.9 keV/particle, but the real value is likely to be significantly larger.

8 LIMITATIONS OF THE MODEL

In our model, we make the approximation that the excess specific energy of a gas halo is equal to the total energy injected over the history of the gas. i.e.

$$E_{\text{excess}} \approx \frac{1}{M_{\text{gas}}} \iint \Gamma dV dt, \quad (13)$$

where M_{gas} is the mass of gas in the halo and Γ is the net heating rate per unit volume. Γ thus includes heating by supernovae and active galactic nuclei, and accounts for the energy lost through radiative cooling. We refer to Γ simply as the rate of non-gravitational heating. The volume integration is made over all the gas that later forms the gas halo, thus the volume itself is irregular and varies with time.

However, there are mechanisms other than Γ that can affect the final value of E_{excess} and hence warrant at least a mention. In what follows, we consider a single halo and the evolution leading

up to its virialization. We use the term ‘proto-halo’ to refer to the contents of this halo at all times earlier than virialization (note that the proto-halo is not a halo itself, but can contain progenitor halos).

Briefly, the mechanisms are:

- (i) If the evolution of the gas distribution (which otherwise traces the DM distribution fairly well) is changed significantly by non-gravitational processes, then there can be a ‘gravitational’ contribution to E_{excess} .
- (ii) If the gas pressure outside the proto-halo is raised significantly due to heating, then the work it does on the proto-halo may need to be included.
- (iii) In any progenitor halo that contains hot gas, work is done (by the remaining gas) on gas cooling out near the centre. This has the effect of reducing E_{excess} .
- (iv) Gas that cools out to form BDM and stars is generally located in positions of minimum potential. Removal of this gas may therefore increase the average energy of the remaining gas.

The mechanisms have been listed in order of increasing sophistication in the arguments required. We consider each of them below and attempt to quantify their effects on E_{excess} . We shall also give a more formal definition of E_{excess} and discuss the evolution of E_{gas} in some detail. For definiteness, we shall base our discussions on the halo of a cluster, but they can be easily generalised to smaller halos. The discussion of mechanism (iv) is continued in section 9.4, where it is considered as a candidate for breaking the self-similarity of clusters.

Quite aside from the effects mentioned above, there remains the possibility that when the excess energy is large, some of the gas that ‘belongs’ to a halo (in our model) may extend beyond r_{200} . Also, there is some uncertainty in the efficiency with which ejected gas recollapses into larger halos. We have assumed that such effects are small in the model.

If the heating of proto-cluster gas is very uneven, e.g. this can occur if gas is heated by the radio jets of AGN (section 9.3), then the gas halo may be partially unbound. If the self-similarity of clusters is broken in this way, then small clusters would have lower gas fractions than large clusters. However, the excess energies required would still be very high. For example, the X-ray luminosity of clusters with $T = 2 \text{ keV}$ are roughly an order of magnitude below the self-similar prediction (when normalized to the largest clusters). Since L_X scales as the gas density squared, we would need to unbind 2/3 of the gas to reduce L_X by an order of magnitude (supposing the shape of the gas density profile remains unchanged). The mean excess specific energy of all the gas is then $\approx 2/3$ of the binding energy of the halo.

8.1 The ‘gravitational’ contribution

We begin with a simplified scenario where no gas is ‘removed’ to form stars and BDM in the proto-halo. We generalize the definition of E_{gas} (equation 5) to apply to the proto-halo at any time, by including the kinetic energy of bulk motion:

$$E_{\text{gas}} \equiv \frac{1}{M_{\text{gas}}} \int \rho_g \left(\frac{3kT}{2\mu m_H} + \frac{1}{2} \mathbf{v}^2 + \phi \right) dV, \quad (14)$$

where \mathbf{v} is the velocity of the gas and the volume of integration is as explained above. At early times, the proto-halo occupies a roughly spherical region, but it later condenses into sheets, filaments and halos. Therefore, as a first approximation the potential ϕ can be calculated from the proto-halo only, ignoring matter outside the proto-halo. We set $\phi = 0$ at infinity. (Using a larger region

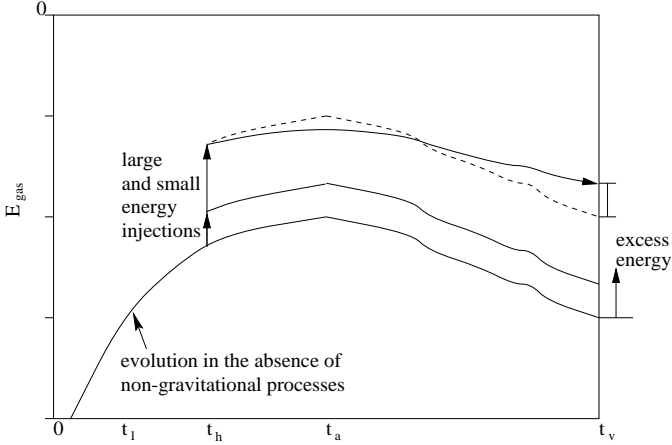


Figure 26. A schematic diagram of the evolution of E_{gas} with time. The times t_h , t_a and t_v give the time of energy injection, the turnaround time and the virialization time respectively. The lowest curve gives the evolution of E_{gas} in the absence of non-gravitational heating or cooling. E_{excess} is defined as the deviation from this curve at t_v . The other two solid curves show the effects of injecting a small and large amount of energy. In the latter case, there is a ‘gravitational contribution’ to the excess energy, given by the difference between the solid and dashed curves at t_v .

to calculate ϕ does not alter our conclusions, but the derivation of equation 17 shall require the above assumption.)

In Appendix B (equation B12) we show that E_{gas} obeys

$$\frac{dE_{\text{gas}}}{dt} = \frac{1}{M_{\text{gas}}} \int \left(\rho_g \frac{\partial \phi}{\partial t} + \Gamma \right) dV, \quad (15)$$

where we have assumed that the gas pressure at the boundary of the proto-halo is negligible. Thus, the rate of change of E_{gas} is given by the net rate of non-gravitational heating, plus a weighted average of $\frac{\partial \phi}{\partial t}$. Since ϕ is dominated by the contribution from DM, we shall make the approximation throughout that ϕ is unchanged by modifications in the gas distribution. This leads to the important observation that the gas processes which drive Γ do not have an immediate effect on the other, gravitational term. (This would not be the case if, for instance, that term included $\frac{\partial \rho_g}{\partial t}$ instead of ρ_g .) This allows us to consider the two terms on the RHS separately.

In the absence of non-gravitational processes (implying $\Gamma = 0$), we expect E_{gas} to increase as the system expands prior to the turnaround time, t_a , and to decrease after t_a . The final value of E_{gas} , at the virialization time t_v , is given by equation 6 in our model. A schematic diagram of this is shown in Fig. 26. Equation 6 itself simply expresses the assumption that the behaviour is self-similar in the absence of non-gravitational processes. (For example, Navarro, Frenk, & White (1995) performed gas and dark matter simulations of the formation of X-ray clusters, with masses from 10^{14} to $2 \times 10^{15} M_{\odot}$. In the absence of non-gravitational cooling or heating, they found similar gas density profiles for all the clusters, and the clusters obeyed the self-similar relation $L_X \propto T^2$.)

The formal definition of E_{excess} is thus the difference between the actual value of E_{gas} at virialization and the value obtained in the absence of non-gravitational processes (given by equation 6). Now suppose the inclusion of non-gravitational heating does not modify the gas distribution at all. In this case, the gravitational term in equation 15 is not affected. E_{excess} is then given by equation 13 exactly, as we have assumed in our model. This is illustrated in Fig. 26 by a single, small injection of energy at time t_h . The subsequent evolution of E_{gas} is unchanged.

If the energy injected is large (comparable to $|E_{\text{gas}}|$), then it can make the gas distribution more extended in the potential well of the proto-halo. This is likely to reduce the magnitude of the gravitational term in equation 15, because more weight is given to areas of smaller $|\phi|$, where $|\partial \phi / \partial t|$ is also likely to be smaller. The total change of E_{gas} between energy injection and virialization is therefore reduced. This is illustrated by the solid curve belonging to the large energy injection in Fig. 26. Its deviation from the dashed curve, which gives the evolution if the gas distribution is not modified, leads to an excess energy that is larger than the energy originally injected. We refer to the difference between the solid and dashed curves at virialization as the ‘gravitational’ contribution to E_{excess} . In general, the gravitational contribution is given by

$$\frac{1}{M_{\text{gas}}} \iint (\rho_g - \rho_{g,G}) \frac{\partial \phi}{\partial t} dV dt, \quad (16)$$

where the subscript ‘G’ means the same system evolved without including non-gravitational processes.

It follows from the above discussion that the gravitational contribution to E_{excess} can be negative if $t_h < t_1$, where t_1 is given by $E_{\text{gas,G}}(t_1) = E_{\text{gas,G}}(t_v)$ (the ‘G’ subscript means the same as before, so that $E_{\text{gas,G}}(t)$ is given by the lowest curve in Fig. 26). In this case, $E_{\text{gas,G}}$ experiences a net *increase* from t_h to t_v , but we expect this net increase to be reduced if the gas is made more extended by heating. As a result E_{excess} is smaller than the energy injected at t_h , if $t_h < t_1$. A crude estimate of t_1 can be obtained with the spherical collapse model by assuming that the radius of the system at t_1 is equal to the virial radius. This gives $t_1 = 0.09t_v$. Since t_1/t_v is small, we expect the bulk of heating to occur after t_1 and hence the gravitational contribution to be positive.

The gravitational contribution to E_{excess} is difficult to estimate in general. Nevertheless, we can consider a somewhat contrived scenario whereby a large injection of energy at time t_h results in a constant value of E_{gas} thereafter. This can occur if all of the gas is pushed outwards to where $\frac{\partial \phi}{\partial t} = 0$, so that the gravitational term in equation 15 vanishes. We expect this to require raising E_{gas} to roughly zero, though it is possible to conceive scenarios which require less energy injection. With the help of Fig. 26, it is then easy to see that the gravitational contribution to E_{excess} is equal to $[E_{\text{gas,G}}]_{t_v}^{t_h}$. It follows that the maximum possible gravitational contribution is obtained by having $t_h = t_a$. We call this E_{max} , where $E_{\text{max}} = [E_{\text{gas,G}}]_{t_v}^{t_a}$.

The distributions of gas and DM are very similar in the absence of non-gravitational processes. If we assume that they are the same, then we can show that the variation of $E_{\text{gas,G}}$ is given by

$$E_{\text{gas,G}} = \frac{1}{M_{\text{gas}}} \int \frac{1}{2} \rho_{g,G} \phi dV + \text{constant}. \quad (17)$$

which is derived in Appendix C. The derivation requires that $\rho_{g,G} = \rho_{\text{tot}} = 0$ outside the proto-halo. Thus,

$$E_{\text{max}} = \frac{1}{M_{\text{gas}}} \left[\int \frac{1}{2} \rho_{g,G} \phi dV \right]_{t_v}^{t_a} \approx \frac{1}{M_{\text{gas}}} \int -\frac{1}{4} \rho_{g,G} \phi dV \Big|_{t_v}. \quad (18)$$

In the approximation we have assumed that the integral scales as the inverse of the radius of the system and that the turnaround radius is twice the virial radius.

In Fig. 26 we have marked intervals of size E_{max} on the E_{gas} -axis. To obtain the absolute value of $E_{\text{gas,G}}$ at t_v , we had to estimate the thermal term in equation 14. We assumed the kinetic term to be zero. The gravitational binding energy of the halo is equal to $\int (1/2) \rho_{\text{tot}} \phi dV$. The virial theorem then implies that the thermal energy of the gas halo is approximately

$f_{\text{gas}}(-1/2) \int (1/2) \rho_{\text{tot}} \phi dV$, where $f_{\text{gas}} = \rho_{\text{g,G}}/\rho_{\text{tot}}$ is a constant and possible boundary terms at r_{200} have been ignored. Dividing by M_{gas} gives the specific thermal energy of the gas: $\int (-1/4) \rho_{\text{g,G}} \phi dV / M_{\text{gas}}$. Therefore,

$$E_{\text{gas,G}}(t_v) \approx \frac{1}{M_{\text{gas}}} \int \frac{3}{4} \rho_{\text{g,G}} \phi dV \Big|_{t_v} \approx -3E_{\text{max}}, \quad (19)$$

as shown in the plot.

As mentioned above, we expect the gas halo to be unbound, so that $E_{\text{excess}} \approx |E_{\text{gas,G}}(t_v)|$, the binding energy of the gas halo. Using the above estimates, it follows that $E_{\text{max}} \approx E_{\text{excess}}/3$, implying a 50 per cent error if E_{excess} is approximated with equation 13. This fractional error will in general be smaller, for $t_h \neq t_a$. Whether similar fractional errors are incurred with less extreme amounts of heating is much harder to determine.

8.2 Work done at the outer boundary

If gas in the proto-halo does work on gas outside, we expect this to reduce E_{gas} , and vice versa. Conceptually, this effect is quite simple, but we need to follow the gas in more detail than before. We introduce the term ‘proto-gas halo’ to refer strictly to the gas which eventually forms the gas halo. Thus it does not include baryons that are incorporated into stars or BDM (or even massive black holes) before virialization. We do not explicitly include gas recycled from stars, which we assume to be small in amount (see also section 2.3). The mass of the proto-gas halo is constant with time.

To distinguish this from our earlier discussion, we introduce e_{gas} to give the total specific energy at a position moving with the gas:

$$e_{\text{gas}} = \frac{3kT}{2\mu m_{\text{H}}} + \frac{1}{2} \mathbf{v}^2 + \phi. \quad (20)$$

Hence, the total energy of the proto-gas halo is $\int e_{\text{gas}} dm = M_{\text{gas}} E_{\text{gas}}$, where we have integrated over the mass of proto-gas halo. In Appendix B, we show that

$$\frac{d}{dt} \int e_{\text{gas}} dm = \int (-P\mathbf{v} + \mathbf{T}\mathbf{v}) \cdot d\mathbf{A} + \int \left(\rho_{\text{g}} \frac{\partial \phi}{\partial t} + \Gamma \right) dV, \quad (21)$$

The only change from equation 15 is an additional surface integral, in which P is the gas pressure, \mathbf{T} is the viscous stress tensor and $d\mathbf{A}$ is a vector element of surface area. The surface integral gives the rate of work done by the proto-gas halo on other gas. The viscous term is almost certainly negligible in what we shall discuss, so we assume that it vanishes. The work done at the outer boundary of the proto-gas halo is then a straightforward integral of PdV .

It is likely that the total work done at the outer boundary is very small. Nevertheless, it is ultimately the change in work done as a result of including non-gravitational processes that we are interested in. Hydrodynamic simulations which do not include non-gravitational heating or cooling result in self-similar X-ray clusters, hence we can be assured that any work done does not prevent them from following a self-similar energy equation (6). The net work done depends on when the heating occurred, since the proto-gas halo expands before contracting. For simplicity, we shall consider the total work done after the turnaround time, to see whether this effect can increase E_{excess} .

We expect most of the work to be done on those parts of the outer boundary which form the ends of filaments and, possibly, the edges of sheets, because density and temperature are highest at these surfaces. Although the rest of the outer boundary has a much

larger area, we shall assume that the pressure there is so small that the work done is not more than that at the end of filaments. For filaments, the volume swept out by the end surfaces should be comparable to the volume of the filaments. This is because infall occurs along the filaments in general. Using the spherical collapse model for comparison, the volume of the sphere at turnaround is $8V_{200}$, where V_{200} is the volume of the virialised halo. Let there be an effective pressure P_{eff} , then the work done on the proto-gas halo between the turnaround time and virialization is $7f_{\text{eff}} V_{200} P_{\text{eff}}$, where $7f_{\text{eff}} V_{200}$ is the effective volume swept out by the said surfaces. Letting $P_{\text{eff}} = \rho_{\text{g,eff}} kT_{\text{eff}} / (\mu m_{\text{H}})$, where we have defined an effective density and temperature, we find that the work done is given by

$$7f_{\text{eff}} V_{200} \frac{\rho_{\text{g,eff}} kT_{\text{eff}}}{\mu m_{\text{H}}} = 7f_{\text{eff}} \frac{\rho_{\text{g,eff}}}{\rho_{\text{g}}} kT_{\text{eff}} \left(\frac{M_{\text{gas}}}{\mu m_{\text{H}}} \right), \quad (22)$$

where $\bar{\rho}_{\text{g}}$ is the mean density of the virialized gas halo and $M_{\text{gas}}/\mu m_{\text{H}}$ is the number of particles in the gas halo. It follows that, the contribution to E_{gas} is equal to

$$7f_{\text{eff}} \frac{\rho_{\text{g,eff}}}{\rho_{\text{g}}} \left(\frac{kT_{\text{eff}}}{\text{keV}} \right) \text{ keV/particle}. \quad (23)$$

The volume filling factor of filaments, which we use to approximate f_{eff} , naturally depends on the threshold density above which we define our filaments. From hydrodynamic simulations of the IGM in a Cold Dark Matter $\Omega = 1$ cosmology (Zhang et al. 1999), threshold overdensities of roughly 1 to 5 (relative to the background baryon density) result in filamentary structures, but higher than ~ 10 , the structures obtained become dominated by knots rather than filaments. Most of the filamentary structures also appear to be in place by $z = 5$, and exhibit mild evolution after that (Zhang et al. 1999). We shall use a fiducial value of $f_{\text{eff}} \sim 0.01$ and a fiducial overdensity of 10. The filaments have typical temperatures of $\sim 10^{-3}$ keV. Since $\bar{\rho}_{\text{g}}$ is 200 times the background density in an $\Omega = 1$ universe, we obtain a fiducial value for the work done on the proto-gas halo of $7 \times 0.01 \times 0.05 \times 10^{-3} = 3.5 \times 10^{-6}$ keV/particle. This is clearly negligible. Even if fairly extreme values of $\rho_{\text{g,eff}}/\bar{\rho}_{\text{g}} = 1/3$ and $kT_{\text{eff}} = 1$ keV (corresponding to strong heating) are used, the work done is only 0.02 keV/particle. It is clear from these values that the work done on the rest of the outer boundary of the proto-gas halo should also be negligible.

8.3 Work done on hot gas that cools

If halos inside the proto-halo (i.e. progenitors of the final halo) contain hot gas that cools out, then work may be done by the proto-gas halo on the gas that cools out. (In cold collapses, very little work is done in this way, as the gas is not pressure-supported in general.) In this case, the total energy of the proto-gas halo is reduced.

Suppose the proto-gas halo has an inner surface or ‘bubble’ that lies inside some progenitor halo that contains hot gas (in reality the ‘bubble’ is likely to be quite irregular). Let ρ_{g} and T be the density and temperature at this surface. Then the work done as the bubble shrinks is $\int PdV = \int kT/(\mu m_{\text{H}}) \rho_{\text{g}} dV$. We shall assume that the gas halo is isothermal. Inside the bubble, the gas that cools out has an initial density that is greater than ρ_{g} at the bubble wall (since its cooling time is shorter). Hence $\rho_{\text{g}} dV$ (calculated at the bubble wall) is an underestimate of the corresponding mass of gas that cooled out. It follows that if we replace $\rho_{\text{g}} dV$ in the integral with dm , the mass of gas that cooled out, then we overestimate the work done. Hence $kT(m_{\text{BDM}}/m_{\text{H}})$ gives an upper limit on the to-

tal work done, where m_{BDM} is the mass of hot gas that cooled out and thus turned into BDM in our model.

There are two points to note about this result. Firstly, the actual fate of the hot gas that cooled is irrelevant: the work done is the same whether it forms BDM, stars or a cold disk. Secondly, if *all* of the hot gas in the progenitor halo cools out, then the ‘bubble wall’ must lie outside the gas halo, where the pressure is probably negligible. This suggests that we should not count such cases at all.

Over the history of the proto-gas halo, the total work done on hot gas that cools out is thus $< \sum kT(m_{\text{BDM}}/m_{\text{H}})$, where the summation is made over all progenitor halos that did not cool out all of their hot gas. The resulting reduction in E_{gas} is therefore smaller than

$$\left(\frac{1}{M_{\text{gas}}}\right) \sum m_{\text{BDM}} \left(\frac{kT}{\text{keV}}\right) \text{ keV/particle.} \quad (24)$$

We have computed this quantity for clusters, using Model B and both sets of parameters given in Table 1. Model B was used because it only requires isothermal gas profiles. The upper limits obtained for small clusters ($T \approx 2$ keV) are in the region of 0.25 keV/particle, with a scatter of 50 per cent either way. The upper limits for large clusters ($T \approx 10$ keV) are roughly twice as large. The two simulations gave similar results. Hence the reduction in E_{gas} is sufficiently small that it should not affect the structure of clusters.

Finally, we note that the bubble is just an imaginary surface for separating different subsets of gas. If heating (in the form of Γ) occurs inside a bubble, gas outside can still be heated via the surface term in equation 21. For most purposes, the distinction is best ignored. Since we only follow the mean excess specific energies of gas halos, excess energy is always, in effect, distributed uniformly throughout a gas halo.

8.4 Selective removal of gas

Having developed the machinery to follow clumps of gas individually, it is natural to ask whether the spatial distribution of gas belonging to the proto-gas halo can itself result in excess energy. This becomes clear if we consider the proto-gas halo at very early times. Its outer boundary is then almost spherical, but it would contain many ‘bubbles’ inside it as explained above. If the bubbles occur preferentially towards the centre of the sphere, then the gas would have positive excess specific energy, because it would be more likely to find gas at larger radii (where ϕ is more positive) compared to a uniform distribution. Again, we are comparing to the case in which non-gravitational processes are not included, when the proto-gas halo is just a uniform sphere at very early times. We discuss why the above scenario is likely to occur in section 9.4.

To calculate the excess energy, it is easier to make comparisons when the halo has virialized, because the time evolution of $\int e_{\text{gas}} dm$ is complicated. Consider a virialized gas halo obtained in the absence of non-gravitational processes: only a subset of its gas particles remain in the gas halo if the system is evolved with non-gravitational processes included, since the rest of the particles form stars and BDM. If the subset of particles has a more extended distribution than all the particles included, then they would have a corresponding excess specific energy (we assume that the gas is isothermal for simplicity). In section 9.4 we estimate excess energies using this method.

The exact value of E_{excess} is thus the sum of all the effects mentioned above, some of which are small. The gravitational contribution is probably the most uncertain as it depends on how the

gas distribution is modified. Note that an estimate obtained using the above method already includes the positive gravitational contribution that results from the subset of gas particles being more extended. This is because the estimate is obtained after virialization, so that the evolution of $\int e_{\text{gas}} dm$ for the subset of gas particles is already accounted for. In fact, the estimate over-compensates for this effect, because gas belonging to the subset would not stay at the same radii when cooling is included, but would gradually fall to smaller radii to replace cooled gas. Hence the method gives a slight over-estimate of the excess energy.

9 BREAKING THE SELF-SIMILARITY OF CLUSTERS

In WFN98 we were able to obtain sufficient excess energy in clusters to match the X-ray data, by making a couple of assumptions. We showed that if most of the iron abundance of intracluster gas originated from type II supernovae (SNII) rather than type Ia supernovae (SNIa) *and* if most of the associated supernova energy (we used $\epsilon_{\text{SN}}=1$) had not been radiated, then the excess energy associated with the observed iron abundance would be ~ 1 keV/particle.

The type of supernova matters because SNIa produce ~ 10 times more iron than SNII, while injecting roughly the same amount of energy. Hence if the iron observed in cluster gas came from SNIa only, the energy injected would be ~ 10 times less. Unfortunately, there is much uncertainty in the fraction of iron contributed by each type of supernova. A recent analysis suggests that the fraction due to SNIa is between 30–90 per cent, depending on the supernova model (Nagataki & Sato 1998).

A more serious problem exists in the assumption that most of the supernova energy is not radiated. Supernovae exploding in cold gas are likely to radiate a large fraction of their energy, thus reducing the value of ϵ_{SN} . Thornton et al. (1998) made a systematic study of supernovae exploding in cold gas (1000 K) in a range of gas densities and metallicities. Using initial supernova energies of 10^{51} erg, they found that in the late stages of evolution supernova remnants had total energies of $\approx (9-30) \times 10^{49}$ erg, depending on the environment. A total energy of 10^{50} erg was considered typical, which corresponds to $\epsilon_{\text{SN}}=0.25$ in our model. In reality the situation is complicated by the inhomogeneity of surrounding gas. Also, if the supernova rate is sufficiently high that remnants overlap before going radiative, then we would expect much higher heating efficiencies. Nevertheless, the above value of ϵ_{SN} agrees remarkably with those shown in Table 1. If gas that is ejected later takes part in cold collapses, then further energy loss would occur (section 6.2).

Below, we investigate four different approaches to breaking the self-similarity of clusters, keeping our discussion as model-independent as possible.

9.1 Supernova heating

As discussed in section 6.2, if gas is ejected from galaxies at no higher than the escape velocity, then the excess specific energies of clusters do not come close to 1 keV/particle, the minimum level required to break their self-similarity (section 7). (If gas is not ejected, then it clearly contributes still less excess energy.) This does not depend on the model of star formation, because the binding energies of halos of $\sim 10^{12} M_{\odot}$ are only a few tenths of keV/particle (Fig. 7)—if star formation ceases in more massive halos then this sets an upper bound on the excess energy of clusters. It is possible to increase slightly the size of halos above which star formation ceases [by increasing τ_0 in our model, limiting circular

velocity in other SAMs (Somerville & Primack 1998)], but this is constrained by the position of the exponential dropoff in galaxy luminosity functions. Therefore, we expect this upper bound to be at most 1 keV/particle. At the very least, the excess energy is then reduced by dilution, since not all of the cluster gas is processed through these largest galaxies.

The halos of groups have higher binding energies and it is possible that some of their cooled gas may be turned into stars. For example, observations suggest that 10–20 per cent of gas which cools in cooling flows may form stars (Cardiel, Gorgas, & Aragon-Salamanca 1998). However, an extreme example demonstrates the futility of this approach. We ran a simulation using Model A and the same parameters given in Table 1, changing only the behaviour of halos in the range $(8\text{--}123) \times 10^{12} M_\odot$. For halos in this range, all of the gas able to cool was allowed to form stars, generating 1 SNII per $16 M_\odot$ of star formation (in this case this includes all stars formed, rather than those below $1 M_\odot$ only). Each supernova released 10^{51} erg, i.e. $\epsilon_{\text{SN}}=2.5$ (as radiative loss is small for supernovae exploding in hot gas), all of which was injected into gas that did not cool. In other words, no negative feedback on the cooling gas was included. The resulting excess energy in clusters of a few $10^{14} M_\odot$ were only ≈ 1 keV/particle. Basically, not enough gas is able to cool in groups, hence groups can be ruled out as the source of the required supernova heating.

If the binding energies of halos below $8 \times 10^{12} M_\odot$ are too low, then how robust is the limit set by binding energy on excess energy? Such a limit is likely whenever star formation is ‘enclosed’ by large amounts of gas, e.g. a hot gas halo or a continuous infall of cooling gas. If supernova ejecta do not have a clear path to infinity, then surrounding gas is heated gradually. In this situation, we expect gas to leave the site of heating as soon as it has sufficient energy to escape the halo: hence the limit.

The time between star formation and supernovae is only $\sim 5 \times 10^6$ years, which is much shorter than the free-fall time of any galaxy halo. Hence in a cold collapse, the bulk of gas in the halo is still falling towards the centre when star formation begins, so that supernovae remain ‘enclosed’. However, because the gas is mostly cold and clumpy, it is possible that a free path may be found for gas to be ejected from the halo at much higher than the escape velocity. This would be aided by aspherical infall of the gas. Alternatively, it may be possible for star formation to be delayed until most of the gas in the halo has settled into a disk, by magnetic pressure, turbulence and/or angular momentum support. In either case, it would be necessary to carve out ‘chimneys’ in the surrounding cold gas in order to allow heated gas to escape easily.

We can thus set out the requirements for a solution that involves supernova heating. From the fiducial parameters used in WFN98, it is clear that the fraction of supernova energy retained in cluster gas must be very high. Even if all the iron in cluster gas originated from SNII, almost all of the approximately 10^{51} erg per SNII needs to be retained in order to achieve close to 2 keV/particle of excess energy. Therefore, hot gas generated by supernovae must escape before going radiative, and escape with excess energies of at least 10, in general ~ 100 times the binding energies of the host halos (in order to achieve excess energies > 1 keV/particle—see Fig. 7). With this excess energy, the heated gas would not take part in further cold collapses. The ejected gas would need to account for a large fraction of gas in the cluster, in order to minimise dilution, otherwise the gas would need to be ejected with correspondingly higher excess energies.

We would expect most of the stars observed in present-day clusters to be formed in such massive outbursts, since we already

require supernova rates that are 5 times higher than obtained from a standard IMF.

It is generally believed that supernovae regulate the amount of star formation in dwarf galaxies. However, the above requirements essentially amount to a decoupling of supernova energy from the bulk of the gas in a cold collapse. There are two aspects to this: firstly, gas that is not being ejected must not receive a large fraction of the energy, otherwise a substantial fraction would be radiated (as the gas is cold), and secondly, since the energy goes into a much smaller quantity of gas, the amount of gas ejected is ~ 100 times less for the same amount of star formation, so that the amount of cold gas available for forming stars changes little. For example, in our model of star formation and feedback, the amount of star formation in dwarf galaxies would be greatly increased, and subsequent (larger scale) collapses would become very gas-deficient (because the ejected gas can only recollapse into a cluster). Thus star formation would be restricted to the smallest halos. To remedy the above, another ‘regulator’ of star formation would be required. For example, in other SAMs (Somerville & Primack 1998) star formation occurs in a cold gas disk, which is converted into stars on a star formation timescale that is parametrised. However, the second problem remains: since much less gas would be ejected from the disk, more cold gas would remain, so that the published star formation timescales would need to be increased in order to give similar amounts of star formation.

Two aspects may help to increase the excess energy, namely the gravitational contribution (section 8.1) and the increased pressure at the outer boundary of the proto-gas halo (section 8.2). More detailed calculations would be required to estimate their contribution.

Our discussion may be altered if hypernovae releasing $\sim 10^{52}$ erg each (Iwamoto et al. 1998) were common. Since the progenitors of hypernovae are believed to be stars of mass $\gtrsim 40 M_\odot$, such a scenario would still require an IMF strongly biased towards very massive stars.

9.2 Pre-collapse gas at high entropy

It was proposed by Kaiser (1991) and (Evrard & Henry 1991) that a better match to the $L_X - T$ relation of X-ray clusters could be obtained if the IGM was ‘preheated’ to a high entropy prior to collapse of the gas. Navarro, Frenk, & White (1995) used this method in hydrodynamic simulations of three clusters, using a gas fraction of 0.1 in an Einstein-de-Sitter universe. By giving all gas particles a uniform high entropy at a redshift of $z = 3$ (no radiative cooling was included), they were able to obtain clusters that closely followed $L_X \propto T^3$. However, the gas profiles of their simulated clusters differed from those originally envisaged by Kaiser, who assumed that the gas would evolve adiabatically after preheating. This simplifies the derivation of the resulting scaling relations, but requires that the entropy be sufficiently high, otherwise shocking-heating would become important. (In the limit of a very low preheated entropy, the entropies in clusters would be completely determined by shock-heating and self-similar behaviour would be recovered.) We have stressed that sufficient excess energy is required in order to match the $L_X - T$ relation, but the problem can be approached differently if it is assumed that gas in all clusters (below a certain mass) has the same preheated entropy. This was studied in detail by Balogh, Babul, & Patton (1999). Using an initial entropy slightly higher than, though marginally consistent with, the observed ‘entropy floor’ (Ponman, Cannon, & Navarro 1999), they found that the isentropic model is able to fit the properties of groups ($T \lesssim 1$

keV) but not clusters. This was attributed to the need for accretion shocks to raise the entropy further in clusters.

Ponman et al. (1999) measured the entropy of gas in clusters at one tenth of the virial radius, just outside any cooling flow regions, and found that the entropies measured in poor clusters and groups were higher than predicted by self-similarity. Instead, the entropies appeared to settle on a lower limit or ‘floor’ given by $T/n_e^{2/3} \sim 100h^{-1/3}$ keV cm². This therefore gives a likely value for the initial entropy in an isentropic model, but more generally implies that the initial entropy should not be any higher. The results of Balogh, Babul, & Patton (1999) agree with our finding in section 7.1, that in order for an isentropic cluster with $T \sim 2$ keV to fit the $L_X - T$ relation, the entropy needs to be roughly 3 times higher than the entropy floor observed by Ponman et al. We also noted that the gas profiles that matched the observed entropies (as well as the $L_X - T$ relation) had γ close to 1 (Fig. 25). Since small values of γ imply steep entropy gradients, this further supports the notion that shock heating is important in small clusters.

The precise mechanism by which an entropy floor may have been created is uncertain (Kaiser 1991). It is often supposed that the gas is heated at low density while in the IGM (Ponman et al. 1999, Balogh et al. 1999), so that the temperature increase required to reach a given entropy is reduced. If supernovae were the source of energy and galactic winds (i.e. shock-heating) the mechanism, then in order for most of the gas that is preheated to receive the energy at low density, the gas ejected from galaxies must form a very small fraction of the preheated gas. This corresponds to the case of high dilution given in section 9.1, and pushes the requirements given there further into the extreme. The energy required to establish the observed entropy floor is at least ~ 0.3 keV/particle (as discussed by Ponman et al. 1999, Balogh et al. 1999), even if the gas is heated at low density. If proto-cluster gas was given thermal energies of ~ 1 keV/particle, then an entropy floor may be likely consequence. However, cooling in clusters may also result in the minimum entropies observed by Ponman et al. (section 9.4).

As regards the modelling of gas halos, the final distribution of gas in a cluster certainly depends on entropy as well as energy (e.g. Bower 1997). In general, the final entropy is the result of virialization shocks. However, if the gas was somehow heated at a very low density with a modest amount of energy, then the resulting entropy may be very high—if this corresponds to a temperature much higher than the virial temperature after adiabatic compression to densities found in the cluster, then the gas distribution would be altered or may not even be bound. However, the minimum density experienced by the gas is limited by the overdensity that led to the cluster in the first place, as well as smaller scale density fluctuations. This is another way of saying that the amount of compression, hence work done on the gas, is limited. Indeed, we have shown that the energy for compressing the gas comes almost completely from gravity rather than pressure on the outside (section 8.2), so that the total energy of the system (gas and dark matter) is roughly conserved.

To estimate the maximum compression ratios for a cluster, we can use the spherical collapse model as a first approximation. The turnaround radius of this sphere is then twice the final virial radius, so that the mean density of the sphere has a minimum equal to 1/8 of the mean density of the virialized halo. This simple model suggests that adiabatic compression can increase the temperature of preheated gas by a factor of 4 at most. Alternatively, we can compare the minimum density obtained above to a fiducial density of $n_e = 10^{-3}$ cm⁻³ near the centre of a cluster (above which cooling can significantly modify the entropy during the life of the cluster).

The mean gas density at turnaround for a halo that collapses at time t is given by $200f_{\text{gas}}/(48\pi Gt^2)$, where f_{gas} is the gas fraction. This implies an electron density of $n_{e,\text{min}} = 2.0 \times 10^{-5} f_{0.2}/t_{10}^2$ cm⁻³, where $t_{10} = t/(10^{10} \text{ years})$ and $f_{0.2} = f_{\text{gas}}/0.2$. Thus the temperature increase when this gas is compressed to density $n_e = 10^{-3}$ cm⁻³ is a factor of $13t_{10}^{4/3}(n_{-3}/f_{0.2})^{2/3}$, where $n_{-3} = n_e/(10^{-3} \text{ cm}^{-3})$. In reality, this factor is much reduced by clumping of the gas into filaments and sheets by the turnaround time, so that typical value of $n_{e,\text{min}}$ should be much higher than we have estimated. In addition, the central region of the cluster, with roughly the fiducial density of $n_e = 10^{-3}$ cm⁻³, almost certainly virialized at an earlier time as a less massive halo. If this virialization time is used in t_{10} and filamentary nature of the gas at turnaround is accounted for, then the temperature increase due to adiabatic compression is only a factor of a few.

Suppose the maximum temperature increase is a factor of 4, and gas associated with the core of a future cluster or group is heated at turnaround to a temperature of 0.1 keV, then adiabatic compression would raise this to 0.4 keV. This would still only affect the structure of groups. For the above to occur, the heating would also have to be concentrated around the turnaround time. Since the core of a cluster virializes at an early time, the corresponding period of turnaround is short and occurs at high redshift.

9.3 Heating by active galactic nuclei

Energetically speaking, the total energy released in the formation of massive black holes at the centres of galaxies is sufficient to heat all the baryons in the universe to very high excess energies. However, the main difficulty and uncertainty lies in dissipating this energy into the gas: this may occur through jets and winds, but the energy released in this form is uncertain, while the energy released as radiation is relatively well measured. Ensslin et al. (1998) estimated the total energy released by black hole formation in the Coma cluster. They assumed a mass-to-light conversion rate of $\epsilon \approx 0.1$ and roughly the same rate of energy release in relativistic particles and magnetic fields (as in the jets of radio galaxies). The total energy released in the latter form was found to be comparable to the thermal energy of gas in the Coma cluster.

From the observed luminosity density of AGN, the total mass density of black holes in the universe can be estimated (Soltan 1982; Chokshi & Turner 1992; Fabian & Iwasawa 1999). Using the X-ray background intensity at 30 keV, Fabian & Iwasawa (1999) recently estimated the black hole density in the universe to be $6-9 \times 10^5 M_\odot \text{ Mpc}^{-3}$. This is higher than earlier estimates that used optical counts of AGN (Soltan 1982; Chokshi & Turner 1992), which were likely to suffer from strong intrinsic absorption (Fabian et al. 1998). Assuming a mass-to-light conversion rate of 0.1 and a black hole density of $6 \times 10^5 M_\odot \text{ Mpc}^{-3}$, the total energy radiated by AGN is then $6.4 \times 10^{58} \text{ erg Mpc}^{-3}$. If the same amount of energy is available in relativistic particles and magnetic fields and it is divided uniformly over all the baryons in the universe, then we obtain an energy injection of 3.7 keV/particle. We have assumed $\Omega_b = 0.08$ and $h = 0.5$, as in the rest of this paper. This would be more than enough to break the self-similarity of clusters in our model (Table 2). On the downside, we note that only about 10 per cent of AGN have observed radio jets. If such jets provide the only mechanism for AGN to heat surrounding gas, then the estimated excess energy would be correspondingly reduced. However, it is possible that radio-quiet quasars may provide substantial amounts of excess energy to surrounding gas through outflows of thermal gas

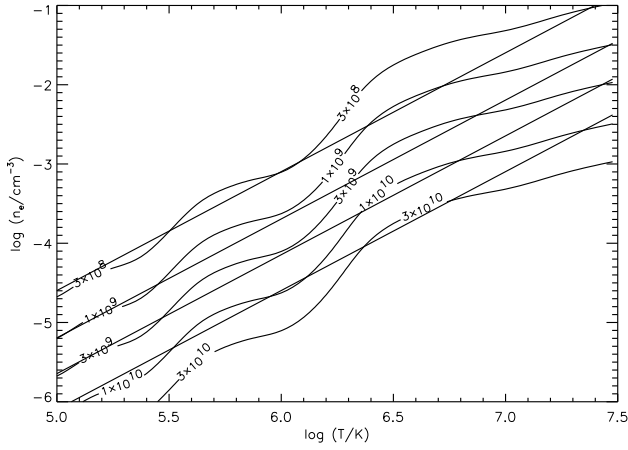


Figure 27. Contour plot of cooling time and entropy in phase space. A metallicity of 0.3 solar (roughly the metallicity observed in cluster gas) was used in the cooling function of Böhringer & Hensler (1989). The contours of cooling time are labelled in years. The straight lines are contours of entropy. From the bottom upwards, they are $T/n_e = 100, 50, 25, 10$ keV cm². Notice that, especially for $T < 10^6$ K, the two sets of contours roughly follow each other.

and poorly-collimated ‘jets’ of radio-emitting plasma (see Kuncic 1999 and references therein).

9.4 Selective removal of gas by cooling

As explained in section 8.4, it is possible that the removal of gas that cools can result in an excess specific energy in the remaining gas that finally forms the intra-cluster medium. We begin by considering whether cooling can also break the self-similarity of the entropy of small clusters, as observed by Ponman et al. (1999). Fig. 27 shows a contour plot of cooling time and entropy in the phase space of gas density and temperature, assuming a metallicity of 0.3 solar (roughly the metallicity observed in cluster gas). The plot shows that the contours of cooling time roughly follow the contours of entropy, though there are slight shifts with temperature. Hence if a gas halo is allowed to cool for a certain period of time, all the gas below a corresponding entropy would cool out. If gas below an entropy of ~ 100 keV cm² is removed by the present day, then the entropy of small clusters would not fall below this level.

Although the cooling times required ($\sim 10^{10}$ years) are long, the cooling begins long before most of the cluster is assembled. Consider tracing the history of the ‘proto-cluster’ backwards in time such that at each merger only the largest progenitor is followed (see for example Navarro, Frenk, & White 1995, Fig. 3). If the largest progenitor in any merger contains hot gas, then this gas is likely to end up at the centre of the new gas halo. Shock heating of the gas near the centre tends to be weak. Gas from the other halo(s) in the merger tend to make up the outer parts of the new halo and therefore shock to higher entropies than the gas at the centre. The same applies to accretion of smaller clumps of gas. Therefore, as gas at the centre of the proto-cluster cools out, the entropy at the centre increases continuously even through mergers (as long as not all of the hot gas in the halo cools out). The cooling time that should be used in Fig. 27 is therefore the time since hot gas with an entropy of ~ 100 keV cm² first appeared in the progenitor that formed the core of the proto-cluster.

In order to fit the observed $L_X - T$ relation, it is also necessary to have sufficient excess energy. Continuing from section 8.4, this can be estimated from the subset of gas particles, in a cluster evolved in the absence of non-gravitational processes, which remain in the gas halo when the cluster is evolved with radiative cooling included. If the subset has a more extended distribution than all the gas included, then a positive excess energy would result. This would happen if gas at smaller radii had a higher probability of cooling out than gas at larger radii.

The above scenario is likely for the following reason. Theory predicts that the first halos of a given mass to collapse should be much more strongly clustered than the background density distribution (Kaiser 1984). For instance, the large-scale over-densities that created present-day clusters also raised the overall density of smaller-scale fluctuations, so that the first galaxy halos to collapse had a high probability of being associated with future clusters. The above has been used to explain the strong clustering of ‘Lyman-break galaxies’ (LBG) observed at $z \sim 3$ (Steidel et al. 1998; Adelberger et al. 1998; Giavalisco et al. 1998), where good agreement with theoretical predictions have been obtained if the typical LBG is associated with a halo of mass $\sim 10^{12} M_\odot$. N-body simulations show that the densest peaks in the distribution of LBGs are likely to be the progenitors of future clusters (Governato et al. 1998; Wechsler et al. 1998). If we make the reasonable assumption that the large-scale over-density that led to a cluster was highest near the centre, then it seems likely that the LBGs would form preferentially near the centre of the cluster. Naturally, as more of the proto-cluster goes non-linear, galaxies would become more uniformly distributed in the proto-cluster. Nevertheless, the first sub-halos of a given mass to collapse also have the highest mean gas density, so that they have the shortest cooling times. Hence gas is more likely to cool out, and be removed, near the centre of the cluster.

To obtain an upper bound on the excess energy obtainable in this way, we modelled the virialized cluster (with all gas particles included) using singular isothermal spheres ($\rho \propto r^{-2}$) for both the gas and dark matter. Assuming a primordial baryon fraction of 0.27, a cluster gas fraction of 0.17 is obtained if we remove all of the gas inside a radius of $(10/27)r_{200}$ in the above gas distribution. The difference in E_{gas} before and after the gas is removed thus gives the excess energy. Since the gas is isothermal, it is only necessary to calculate the gravitational term in E_{gas} , as the thermal terms cancel when we take the difference. The result is $E_{\text{excess}} = (10/17) \ln(10/27) GM_{\text{tot}}/r_{200} = 0.58 GM_{\text{tot}}/r_{200}$, where M_{tot} is the total mass of the halo. For the cluster displayed in Fig. 24 (which has a virial radius of 1.46 Mpc), this gives a excess energy of 1.4 keV/particle.

In reality the gas removed must be more extended than assumed above. Removing a uniform fraction of gas at each radius naturally leads to no excess energy. If we model the more general case by removing gas in two component: a ‘uniform’ component followed by a component involving all the (remaining) gas inside a radius of fr_{200} , then we get

$$E_{\text{excess}} = -\frac{f \ln f}{1-f} \frac{GM_{\text{tot}}}{r_{200}}. \quad (25)$$

For example, if half of the gas removed is in the uniform component, then $f = 5/(27-5) = 5/22$. This gives $E_{\text{excess}} = 0.44 GM_{\text{tot}}/r_{200}$, or 1.0 keV/particle for the above cluster. Increasing the uniform component to 3/4 of the gas removed, so that $f = 2.5/19.5$, gives $E_{\text{excess}} = 0.30 GM_{\text{tot}}/r_{200}$. This corresponds to 0.7 keV/particle for the above cluster.

We note that the high excess energies required in clusters mean that the gas associated with groups probably have similar excess energies. In this case, the gas distributions in groups would be strongly affected. The amount of gas able to cool out in groups would then be smaller than we have supposed, from our simulations of section 6.

In conclusion, the excess energies obtained from cooling are not sufficient on their own to break the self-similarity of clusters, but they may contribute a sizable fraction of the required excess energy.

10 CONCLUSIONS

We have constructed a self-consistent semi-analytic model (SAM) of galaxy formation which follows the excess energies resulting from supernova heating and radiative cooling. The gas density profiles of virialized halos are chosen according to the excess energy in the gas, from a 2-parameter family of polytropic gas profiles in NFW (1997) potential wells. The main assumption of our model is that in the absence of non-gravitational heating or cooling, the total energy of gas in virialized halos follow a self-similar relation, by scaling as the gravitational energy of the virialized halo (modelled with NFW density profiles). This is motivated by the self-similar gas density profiles obtained in hydrodynamic simulations (Navarro, Frenk, & White 1995). The self-similar relation was normalized by matching the model clusters to the largest observed X-ray clusters. Four contrasting ‘heating models’ have been used, in which gas profiles are modified in different ways in the presence of excess energy. In addition, we have investigated effects not included in the SAM that may also contribute to the excess energy of gas halos.

Our main conclusions are as follows:

- If gas is ejected in galactic winds at the escape velocity of the host halo, then the excess energies obtained in halos of all masses follow a distinct pattern, which is not sensitive to the rate of supernova per unit star formation, nor the efficiency of supernova heating (which we parametrised as ϵ_{SN}).
- In this case, the excess energy in clusters is only ~ 0.1 keV/particle. It is strictly limited by the binding energy of the most massive halos to form stars, which are a few $10^{12} M_{\odot}$ in most SAMs.
- Roughly half of the supernova energy injected into proto-cluster gas was found to be radiated when the gas took part in subsequent cold collapses. This energy loss is in addition to the energy radiated immediately following the supernova explosions.
- The main effect of the excess energies on isolated galaxies was to roughly halve the fraction of gas able to cool in halos of $10^{12} - 10^{13} M_{\odot}$, and to shift the transition from cold to hot collapse to less massive halos. Omitting the effect of excess energy on gas density profiles led to a massive increase of star formation in the above range of halos.
- The effect of excess energy on galaxies which experience cold collapse is small.
- The excess specific energies required to break the self-similarity of X-ray clusters and match the observed $L_X - T$ relation were found to be in the range 1.8–3.0 keV/particle. This is the range spanned by the different values obtained using each of the four contrasting heating model. Loewenstein (1999) required similar amounts of heating to fit other properties of X-ray clusters.
- More detailed analysis of a fiducial cluster with $T \approx 2$ keV,

virializing at $z = 0$, showed that the minimum excess energy required was 0.9 keV/particle when all available gas profiles were considered. The gas halo in this case has a uniform entropy that is roughly 3 times too high compared to the entropy measurements of Ponman et al. (1999). Thus the excess specific energy is unlikely to be this low in reality.

- If the gas distribution in the proto-cluster is significantly modified by non-gravitational heating, then there may be a positive ‘gravitational’ contribution to the final excess energy. This could assist in breaking the self-similarity of X-ray clusters.
- The amount of work done on proto-cluster gas by the pressure of gas that does not belong to the final intra-cluster medium is too small to affect the properties of the final X-ray cluster.
- If supernovae are the source of most of the excess energy in clusters, then a very contrived scenario is required in which galaxies ejected gas at extremely high energies (~ 100 times the binding energy of the halo would be typical), and in which supernovae would be much diminished in their role as regulators of star formation. In addition, the bulk of the iron observed in intra-cluster gas would have to be due to Type II supernovae.
- We confirm that establishing an entropy floor of $T/n_e^{2/3} \sim 100$ keV cm² (Ponman et al. 1999) is on its own insufficient to break the self-similarity of clusters (Balogh et al. 1999). Sufficient excess energy is required in order for clusters to match the $L_X - T$ relation.
- The recent estimate of the black hole density in the Universe (Fabian & Iwasawa 1998) implies that there is sufficient AGN power to break the self-similarity of clusters, assuming that the energy released in relativistic particles and magnetic field is similar to that radiated. However, the mechanism for dissipating this energy in proto-cluster gas is uncertain.
- A sizable fraction of the excess energies of clusters may be due to the preferential removal of cooled gas near the centre, where the potential is most negative.

We have therefore identified a number of candidates for providing the excess energy required in clusters. However, no one candidate appears to be a likely solution on its own. This increases the likelihood that a combination of heating mechanisms is required.

It seems likely that similar excess specific energies to those required in clusters would be found in groups, in which case a significant fraction of the gas belonging to groups would be unbound. This may also explain their steeper $L_X - T$ relation (see also Balogh et al. 1999). Measurements of the gas distribution and temperature in groups with future satellites such as XMM would clarify many of these issues.

ACKNOWLEDGEMENTS

KKSW thanks Vince Eke, Stefano Ettori, Martin Haehnelt, Fraser Pearce, Clovis Peres, Martin Rees, Joop Schaye and Tom Theuns for helpful discussions. KKSW is grateful to the Croucher Foundation for financial support. ACF thanks the Royal Society for support.

REFERENCES

- Adelberger K. L., Steidel C. C., Giavalisco M., Dickinson M., Pettini M., Kellogg M., 1998, *ApJ*, 505, 18
- Allen C., 1976, *Astrophysical quantities*. Athlone Press, London
- Allen S. W., Fabian A. C., 1998a, *MNRAS*, 297, L57

Allen S. W., Fabian A. C., 1998b, MNRAS, 297, L63
 Arnaud M., Rothenflug R., Boulade O., Vigroux L., Vangioni-Flam E., 1992, A&A, 254, 49
 Balogh M. L., Babul A., Patton D. R., 1999, MNRAS, in press (astro-ph/9809159)
 Baugh C. M., Cole S., Frenk C. S., Lacey C. G., 1998, ApJ, 498, 504
 Benson A. J., Bower R. G., Frenk C. S., White S. D. M., 1999, MNRAS, submitted (astro-ph/9903179)
 Böhringer H., Hensler G., 1989, A&A, 215, 147
 Bower R. G., 1997, MNRAS, 288, 355
 Brighenti F., Mathews W. G., 1998, ApJ, accepted (astro-ph/9811258)
 Burles S., Nollett K. M., Truran J. N., Turner M. S., 1999, Phys. Rev. Lett., submitted (astro-ph/9901157)
 Burles S., Tytler D., 1998, ApJ, 499, 699
 Cardiel N., Gorgas J., Aragon-Salamanca A., 1998, MNRAS, 298, 977
 Cavaliere A., Menci N., Tozzi P., 1997, ApJ, 484, L21
 Chokshi A., Turner E. L., 1992, MNRAS, 259, 421
 Cole S., Aragón-Salamanca A., Frenk C. S., Navarro J. F., Zepf S. E., 1994, MNRAS, 271, 781
 Cole S., Kaiser N., 1988, MNRAS, 233, 637
 David L. P., Slyz A., Jones C., Forman W., Vrtilik S. D., 1993, ApJ, 412, 479
 Ebeling H., Edge A. C., Fabian A. C., Allen S. W., Crawford C. S., 1997, ApJ, 479, L101
 Edge A. C., Stewart G. C., Fabian A. C., Arnaud K. A., 1990, MNRAS, 245, 559
 Elbaz D., Arnaud M., Vangioni-Flam E., 1995, A&A, 303, 345
 Ensslin T. A., Wang Y., Nath B. B., Biermann P. L., 1998, A&A, 333, L47
 Ettori S., Fabian A. C., 1999, MNRAS, 305, 834
 Evrard A. E., 1997, MNRAS, 292, 289
 Evrard A. E., Henry J. P., 1991, ApJ, 383, 95
 Ezawa H. et al., 1997, ApJ, 490, L33
 Fabian A. C., 1994, ARA&A, 32, 277
 Fabian A. C., Barcons X., Almaini O., Iwasawa K., 1998, MNRAS, 297, L11
 Fabian A. C., Iwasawa K., 1999, MNRAS, 303, L34
 Fabian A. C., Nulsen P. E. J., 1994, MNRAS, 269, L33
 Fukazawa Y., Makishima K., Tamura T., Ezawa H., Xu H., Ikebe Y., Kikuchi K., Ohashi T., 1998, PASJ, 50, 187
 Giavalisco M., Steidel C. C., Adelberger K. L., Dickinson M. E., Pettini M., Kellogg M., 1998, ApJ, 503, 543
 Governato F., Baugh C. M., Frenk C. S., Cole S., Lacey C. G., Quinn T., Stadel J., 1998, Nat, 392, 359
 Guiderdoni B., Hivon E., Bouchet F. R., Maffei B., 1998, MNRAS, 295, 877
 Iwamoto K. et al., 1998, Nat, 395, 672
 Kaiser N., 1991, ApJ, 383, 104
 Kauffmann G., Charlot S., 1998, MNRAS, 294, 705
 Kauffmann G., White S. D. M., Guiderdoni B., 1993, MNRAS, 264, 201
 Kuncic Z., 1999, PASP, accepted (astro-ph/9905092)
 Loewenstein M., 1999, ApJ, submitted
 Markevitch M., Forman W. R., Sarazin C. L., Vikhlinin A., 1997, ApJ, submitted (astro-ph/9711289)
 Metzler C. A., Evrard A. E., 1994, ApJ, 437, 564
 Nagataki S., Sato K., 1998, ApJ, 504, 629
 Navarro J. F., Frenk C. S., White S. D. M., 1995, MNRAS, 275, 720
 Navarro J. F., Frenk C. S., White S. D. M., 1997, ApJ, 490, 493
 Nulsen P. E. J., Barcons X., Fabian A. C., 1998, MNRAS, 301, 168
 Nulsen P. E. J., Fabian A. C., 1995, MNRAS, 277, 561
 Nulsen P. E. J., Fabian A. C., 1997, MNRAS, 291, 425
 Peres C. B., Fabian A. C., Edge A. C., Allen S. W., Johnstone R. M., White D. A., 1998, MNRAS, 298, 416
 Ponman T., Cannon D. B., Navarro J. F., 1999, Nat, 397, 135
 Postman M., Geller M. J., 1984, ApJ, 281, 95
 Renzini A., Ciotti L., D'Ercole A., Pellegrini S., 1993, ApJ, 419, 52
 Soltan A., 1982, MNRAS, 200, 115
 Somerville R. S., Primack J. R., 1998, MNRAS, submitted (astro-ph/9802268)

Steidel C. C., Adelberger K. L., Dickinson M., Giavalisco M., Pettini M., Kellogg M., 1998, ApJ, 492, 428
 Thomas P. A., Fabian A. C., 1990, MNRAS, 246, 156
 Thornton K., Gaudlitz M., Janka H.-T., Steinmetz M., 1998, ApJ, 500, 95
 Wechsler R. H., Gross M. A. K., Primack J. R., Blumenthal G. R., Dekel A., 1998, ApJ, 506, 19
 White S. D. M., Frenk C. S., 1991, ApJ, 379, 52
 White S. D. M., Navarro J. F., Evrard A. E., Frenk C. S., 1993, Nat, 366, 429
 Wu K. K. S., Fabian A. C., Nulsen P. E. J., 1998, MNRAS, 301, L20 (WFN98)
 Zhang Y., Meiksin A., Anninos P., Norman M. L., 1999, ApJ, accepted

APPENDIX A: FORMULAE FOR MODELLING THE GAS PROCESSES

The equations used to model the gas processes described in section 2 are given below, along with formulae for some observed quantities. Where required, we assume polytropic gas profiles in NFW potential wells, as derived in sections 3 and 4.1. We remind the reader that the gas profiles used in the formulae are notional, as explained in section 2.2. To denote radius we use r and x interchangeably, where r is the physical radius and $x = r/r_s$.

In this paper, we only calculate the quantities L_X , \dot{M} , emission-weighted temperature and cooling flow power at $z = 0$, for hot gas halos found at this redshift. We therefore take into account any evolution in these quantities over the life of a halo.

A1 The extent of cold gas, x_{CF}

When a new halo forms, the ratio between the cooling time and the free-fall time to the centre of the halo, $\tau = t_{cool}/t_{ff}$, determines whether gas is able to form a hot hydrostatic atmosphere. A hot gas halo forms when $\tau > \tau_0$, where τ_0 is a parameter of the model. If $\tau < \tau_0$ then the gas remains cold in general (as virialization shocks would be radiative and any heating would be transitory). When τ is greater or less than τ_0 everywhere, the above criteria are simple to apply. Otherwise, if τ increases monotonically with radius, then there is a unique radius, x_{CF} , where $\tau = \tau_0$. Gas inside of x_{CF} is then classified as cold and the remaining gas forms a hot gas halo. In all cases, our model requires that there be one radius x_{CF} lying in the range 0 to c , for the purpose of classifying gas as hot or cold. Since $\tau(x)$ is comparable to τ_0 in a narrow range of halo masses (corresponding to normal galaxies), the variation of τ with radius is of concern only for this mass scale. For this reason we will only discuss in detail gas profiles used in section 6 (i.e. those belonging to Models A and B). We first derive the general expression for $\tau(x)$ before considering less well-behaved cases.

The cooling time of gas is given by

$$t_{cool} = \frac{3}{2} \frac{\rho_g kT / \mu m_H}{n_e n_H \Lambda(T)}, \quad (A1)$$

where ρ_g , T , n_e and n_H (the electron and hydrogen number densities respectively) are all functions of r . The three densities are simply proportional to each other. The cooling rate is given by $n_e n_H \Lambda(T)$, where $\Lambda(T)$ is the cooling function. We use the cooling function of Böhringer & Hensler (1989), which depends on metallicity as well as temperature. We assume that the metallicity of every gas halo is constant with radius. A simple estimate of t_{ff} is obtained by computing the free-fall time for a test particle to reach the centre of a sphere of uniform density:

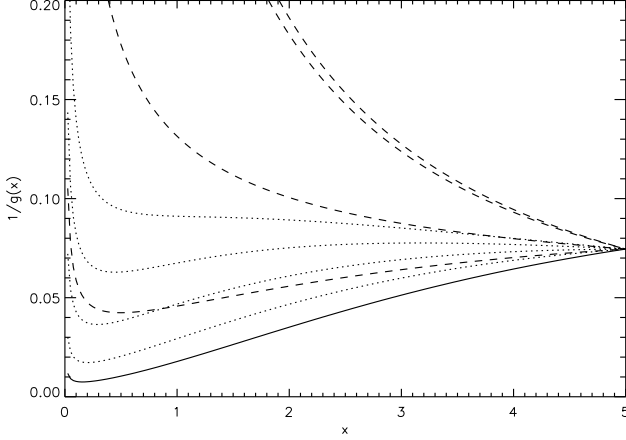


Figure A1. Plot of $1/g(x)$ (which is roughly proportional to $\tau(x)$), the same parameters and linestyles as in Fig. 2. The solid curve is given by $\gamma = 1$ and $\eta_{200} = 10$; the dotted curves are obtained by reducing η_{200} , as in Model B, and the dashed curves by increasing γ , as in Model A (see text for discussion).

$$t_{\text{ff}} = \sqrt{\frac{3\pi}{16G\rho_{\text{tot}}}}, \quad (\text{A2})$$

where ρ_{tot} , the total density of the halo at the radius concerned, has been substituted for this density. (The formula given is a factor of $\sqrt{2}$ greater than that for a collapsing sphere of uniform density.) This method does not account for the increased ρ_{tot} towards the centre of the halo, hence it is a slight overestimate.

It follows that

$$\tau = \frac{t_{\text{cool}}}{t_{\text{ff}}} = \left(\frac{3}{2} \sqrt{\frac{16G}{3\pi}} \frac{\rho_g^2}{n_e n_H} \right) \frac{\alpha}{\eta_{200}} \frac{T}{T_{200}} \frac{\rho_{\text{tot}}^{1/2}}{\Lambda(T)\rho_g}, \quad (\text{A3})$$

where we have used the expressions $\eta_{200} = \alpha\mu m_H/(kT_{200})$ and $\alpha = 4\pi G\rho_s r_s^2$, the latter being the characteristic potential of the NFW profile. We assume a primordial composition of 0.9 hydrogen to 0.1 helium by *number*, which gives $\mu = 0.619$ and $\rho_g^2/(n_e n_H) = 1.707m_H^2$. Expanding $\rho_{\text{tot}}(x)$ and $\rho_g(x)$, we obtain

$$\tau(x) = \left(\frac{3}{2} \sqrt{\frac{16G}{3\pi}} \frac{\rho_g^2}{n_e n_H} \right) \frac{\alpha\rho_s^{1/2}}{\eta_{200}\rho_{g,200}} \frac{1}{\Lambda(T)g(x)}, \quad (\text{A4})$$

where we have defined

$$g(x) = x^{1/2}(1+x) \times \left[1 + \frac{\gamma-1}{\gamma}\eta_{200} \left(\frac{\ln(1+x)}{x} - \frac{\ln(1+c)}{c} \right) \right]^{\frac{1}{\gamma-1}-1} \quad (\text{A5})$$

If $0 < x_{\text{CF}} < c$, then the equation $\tau(x_{\text{CF}}) = \tau_0$ is solved numerically.

To obtain x_{CF} , the model follows an algorithm which first determines whether or not $\tau(x)$ is ‘well-behaved’. This is done by first approximating it as proportional to $1/g(x)$. Although $\Lambda(T)$ is a complicated function when considered over several decades of temperature, the amount that T can vary in a given halo is limited. The steepest temperature profile we use that may be of concern is given by $\gamma = 5/3$ and $\eta_{200} \approx 10$, which is used in Model A. Here the temperature rises by about a factor of 3.5 from r_{200} to the centre. In general, the temperature range in a halo is much smaller, so that the mean variation of $\Lambda(T)$ in halos is not large.

In Fig. A1 we illustrate the general behaviour of $1/g(x)$, using $c = 5$ and the same values as in Fig. 2 for γ and η_{200} . The qualitative behaviour is the same for other values of c . For small enough x , $1/g(x)$ always diverges. This is simply due to the divergence of the NFW density profile and as long as the minimum occurs at sufficiently small x , as with the solid curve ($\gamma = 1$ and $\eta_{200} = 10$), it is ignored. As we decrease η_{200} or increase γ , the minimum moves to larger radii and $1/g(x)$ becomes a flatter function. Eventually, the minimum disappears and if γ is large, $1/g(x)$ becomes a steep decreasing function of x .

Since τ and its interpretation are approximate, we use an algorithm which is relatively simple. The criteria for whether $1/g(x)$ is well-behaved is given by its slope at $x = 0.5$. When this slope is positive (the well-behaved case), $1/g(x)$ is sure to have a minimum inside $x = 0.5$. If $\tau > \tau_0$ at this minimum, then $x_{\text{CF}} = 0$; if $\tau(c) < \tau_0$, then $x_{\text{CF}} = c$; otherwise, $\tau(x_{\text{CF}}) = \tau_0$ is solved numerically.

When this slope is negative instead, $1/g(x)$ is either relatively flat or strongly decreasing at larger radii (see Fig. A1; note that the latter occurs in Model A but not Model B). In this case, if $\tau(0.5) > \tau_0$ ($x = 0.5$ being where the slope is measured), then $x_{\text{CF}} = 0$ and all the gas is considered hot. We have made the assumption that even if $\tau < \tau_0$ at larger radii, there is sufficient hot gas in the centre to provide a working surface on which infalling gas can shock to high temperatures, so that a hydrostatic atmosphere can still form (as discussed in section 2). If $\tau(0.5) < \tau_0$, then $x_{\text{CF}} = c$ and all the gas is considered cold. (For completeness, the algorithm actually allows for the situation, very rare in Models A and B, when $\tau(c) > \tau(0.5)$ in a ‘poorly-behaved’ halo. In this case, it finds a numerical solution if τ_0 lies between $\tau(0.5)$ and $\tau(c)$.)

A2 The fraction, f_{unbind} , of cold gas that forms stars

Supernova feedback from star formation is assumed to eject the rest of the gas once there is sufficient energy to do so. The fraction, f_{unbind} , of cold gas that forms stars is given by,

$$f_{\text{unbind}} \frac{M_{\text{gas}}(x < x_{\text{CF}})}{M_{\text{SN}}} \epsilon_{\text{SN}} 4 \times 10^{50} \text{ erg} = M_{\text{gas}}(x > x_{\text{CF}}) |E_{\text{gas}}| + (1 - f_{\text{unbind}}) M_{\text{gas}}(x < x_{\text{CF}}) |E_{\text{cold}}|, \quad (\text{A6})$$

where M_{gas} is the total gas mass in the specified region and M_{SN} is the mass of stars formed per resulting Type II supernova. For a standard IMF $M_{\text{SN}} = 80 M_{\odot}$ (Thomas & Fabian 1990). Since we boost supernova rates by a factor of 5, $M_{\text{SN}} = 16 M_{\odot}$ in this paper. The energy released by one supernova into surrounding gas is $\epsilon_{\text{SN}} 4 \times 10^{50} \text{ erg}$. E_{gas} is defined in equation 5 and E_{cold} is defined as for E_{gas} except that the thermal term is set equal to zero. $|E_{\text{gas}}|$ and $|E_{\text{cold}}|$ are average quantities which estimate the energies per unit mass required to eject the hot and cold gas respectively.

If the solution to f_{unbind} in the above equation is greater than 1, then the gas halo is not ejected. In this case all the cold gas is able to form stars and $f_{\text{unbind}} = 1$.

A3 The mass of BDM that forms from hot gas

Whenever there is hot gas in a halo, some of it may be able to cool to form baryonic dark matter (BDM) before the next collapse. The cooling radius, r_{cool} , is obtained by solving numerically the equation:

$$\frac{3}{2} \frac{\rho_g kT / \mu m_H}{n_e n_H \Lambda(T)} \bigg|_{r=r_{\text{cool}}} = \Delta t, \quad (\text{A7})$$

where the LHS is the cooling time and Δt is the time from virialization to the next collapse or the present day, whichever is sooner.

The mass of BDM formed is equal to the mass of gas inside r_{cool} minus the mass which has already formed stars, if any. Sometimes no hot gas is able to cool in the given time, in which case no cooling flow operates.

A4 The mass cooling rate, \dot{M}

The instantaneous mass cooling rate, \dot{M} , is estimated using

$$\dot{M} = \left. \frac{dM_{\text{gas}}(r)}{dr} \right|_{r=r_{\text{cool}}} \left. \frac{dr_{\text{cool}}(t)}{dt} \right|_{t=\Delta t}, \quad (\text{A8})$$

where $M_{\text{gas}}(r)$ is the gas mass inside a radius of r , t is the time since the virialization and Δt is as defined above. The cooling radius as a function of t , $r_{\text{cool}}(t)$, is obtained by substituting t for Δt in equation A7.

By differentiating equation A7 with respect to r_{cool} , we obtain

$$\frac{dt}{dr_{\text{cool}}(t)} \approx \frac{3}{2} \frac{\rho_g^2}{n_e n_H} \frac{\alpha}{\eta_{200} \rho_{g,200} r_s \Lambda(T)} \frac{d}{dx} \left(\frac{T \rho_{g,200}}{T_{200} \rho_g} \right), \quad (\text{A9})$$

where we have assumed that $d\Lambda(T)/dr$ is small. Expanding the derivative gives

$$\frac{d}{dx} \left(\frac{T \rho_{g,200}}{T_{200} \rho_g} \right) = \frac{\gamma - 2}{\gamma} \eta_{200} \frac{\rho_{g,200}}{\rho_g} \left(\frac{1}{x(1+x)} - \frac{\ln(1+x)}{x^2} \right). \quad (\text{A10})$$

Since $dM_{\text{gas}}(r)/dr = 4\pi\rho_g(r)r^2$, it follows that

$$\dot{M} = 4\pi \frac{2}{3} \frac{n_e n_H}{\rho_g^2} \frac{r_s^3 \rho_{g,200}^2}{\alpha} \frac{\gamma}{\gamma - 2} \frac{x^2 (\rho_g / \rho_{g,200})^2 \Lambda(T)}{\left(\frac{1}{x(1+x)} - \frac{\ln(1+x)}{x^2} \right)} \Big|_{x=x_{\text{cool}}}. \quad (\text{A11})$$

A5 The cooling flow power

The cooling flow power is the bolometric luminosity of the cooling flow region. It is given by

$$\frac{5}{2} \frac{\dot{M} k T(r=r_{\text{cool}})}{\mu m_H}, \quad (\text{A12})$$

which uses the enthalpy, $5kT/(2\mu m_H)$, to estimate the total energy radiated per unit mass. It corresponds observationally to the bolometric luminosity inside the cooling radius.

A6 The X-ray luminosity, L_X

This is the sum of the cooling flow power and the bolometric luminosity due to the gas outside r_{cool} :

$$L_X = \int_{r_{\text{cool}}}^{r_{200}} n_e n_H \Lambda(T) 4\pi r^2 dr + \frac{5}{2} \frac{\dot{M} k T(r=r_{\text{cool}})}{\mu m_H}. \quad (\text{A13})$$

By the time of observation, the density profile of gas that belonged to $r < r_{\text{cool}}$ differs substantially from that of the notional gas profile due to the effects of radiative cooling. Hence the cooling flow power is estimated separately. Although the changes due to cooling are also felt outside r_{cool} , because volume is a rapidly increasing function of the radius, the effect is only significant close to r_{cool} , so that we treat the atmosphere as unmodified from the notional gas profile outside r_{cool} .

A7 The emission-weighted temperature

This is the temperature that is implied whenever we refer to the temperature of a cluster as a whole (as in section 7). We calculate the temperature as weighted by the luminosity outside r_{cool} . It is thus given by

$$T_{\text{ew}} = \frac{\int_{r_{\text{cool}}}^{r_{200}} T(r) n_e n_H \Lambda(T) 4\pi r^2 dr}{\int_{r_{\text{cool}}}^{r_{200}} n_e n_H \Lambda(T) 4\pi r^2 dr}. \quad (\text{A14})$$

APPENDIX B: GAS ENERGY EQUATION

We derive below the equations that govern E_{gas} and e_{gas} . E_{gas} , defined in equation 14, is the mean total specific energy of gas in a proto-halo. The definitions of proto-halo and proto-gas halo are given in section 8. We use e_{gas} (equation 20) to follow the total specific energy of the gas at a position which moves with the gas.

The gas equations may be written

$$\frac{\partial \rho_g}{\partial t} + \nabla \cdot \rho_g \mathbf{v} = 0, \quad (\text{B1})$$

for the conservation of mass,

$$\rho_g \frac{d\mathbf{v}}{dt} = -\nabla P + \nabla \cdot \mathbf{T} - \rho_g \nabla \phi, \quad (\text{B2})$$

for the conservation of momentum and

$$\rho_g T \frac{dS}{dt} = \sum_{i,j=1}^3 T_{ij} \frac{\partial v_i}{\partial x_j} + \Gamma, \quad (\text{B3})$$

for the conservation of energy. Here ρ_g , T , P , S and \mathbf{v} are, respectively, the density, temperature, pressure, specific entropy and velocity of the gas, ϕ is the gravitational potential, and \mathbf{T} the viscous stress tensor (with components T_{ij}). The lagrangian time derivative is

$$\frac{d}{dt} = \frac{\partial}{\partial t} + \mathbf{v} \cdot \nabla. \quad (\text{B4})$$

The first term on the right in the energy equation is the viscous heating rate. The second term, Γ , is the net additional heating rate per unit volume due to effects other than adiabatic and viscous heating. Such processes include supernova heating and radiative heat loss.

The specific enthalpy is defined as $H = \epsilon + PV$, where ϵ is the specific energy and $V = 1/\rho_g$ is the specific volume. Using the first law of thermodynamics, $d\epsilon = T dS - P dV$, gives $dH = T dS + V dP$, so that

$$\rho_g \frac{dH}{dt} = \rho_g T \frac{dS}{dt} + \frac{dP}{dt} = \sum_{i,j=1}^3 T_{ij} \frac{\partial v_i}{\partial x_j} + \Gamma + \frac{\partial P}{\partial t} + \mathbf{v} \cdot \nabla P, \quad (\text{B5})$$

where we have used the energy equation (B3) and expanded the lagrangian derivative. Using the momentum equation (B2) to replace ∇P in the last term gives, after some algebra,

$$\rho_g \frac{dH}{dt} = \nabla \cdot (\mathbf{T} \mathbf{v}) + \Gamma + \frac{\partial P}{\partial t} - \rho_g \frac{d}{dt} \frac{1}{2} \mathbf{v}^2 - \rho_g \mathbf{v} \cdot \nabla \phi. \quad (\text{B6})$$

Converting $\mathbf{v} \cdot \nabla \phi$ in the last term into time derivatives of ϕ , and rearranging, we get

$$\rho_g \frac{d}{dt} \left(H + \frac{1}{2} \mathbf{v}^2 + \phi \right) - \frac{\partial P}{\partial t} = \rho_g \frac{\partial \phi}{\partial t} + \nabla \cdot (\mathbf{T} \mathbf{v}) + \Gamma. \quad (\text{B7})$$

Using equation B1 and $\rho_g H - P = \rho_g \epsilon$, this can be rewritten as

$$\frac{\partial}{\partial t} \left[\rho_g \left(\epsilon + \frac{1}{2} \mathbf{v}^2 + \phi \right) \right] + \nabla \cdot \left[\rho_g \mathbf{v} \left(H + \frac{1}{2} \mathbf{v}^2 + \phi \right) \right] =$$

$$\rho_g \frac{\partial \phi}{\partial t} + \nabla \cdot (\mathbf{T}\mathbf{v}) + \Gamma. \quad (\text{B8})$$

Integrating this over a comoving volume V , we get

$$\begin{aligned} \int_V \frac{\partial}{\partial t} \left[\rho_g \left(\epsilon + \frac{1}{2} \mathbf{v}^2 + \phi \right) \right] dV = \\ \int_{\partial V} \left[-\rho_g \mathbf{v} \left(H + \frac{1}{2} \mathbf{v}^2 + \phi \right) + \mathbf{T}\mathbf{v} \right] \cdot d\mathbf{A} \\ + \int_V \left(\rho_g \frac{\partial \phi}{\partial t} + \Gamma \right) dV, \end{aligned} \quad (\text{B9})$$

where $d\mathbf{A}$ is a vector element of surface area. But, for any Q and comoving volume V ,

$$\frac{d}{dt} \int_V Q dV = \int_V \frac{\partial}{\partial t} Q dV + \int_{\partial V} Q \mathbf{v} \cdot d\mathbf{A}, \quad (\text{B10})$$

so that when the partial derivative on the LHS of equation B9 is taken outside the integral, we get extra terms which cancel most of the surface terms, giving

$$\begin{aligned} \frac{d}{dt} \int_V \left[\rho_g \left(\epsilon + \frac{1}{2} \mathbf{v}^2 + \phi \right) \right] dV = \\ \int (-P\mathbf{v} + \mathbf{T}\mathbf{v}) \cdot d\mathbf{A} + \int_V \left(\rho_g \frac{\partial \phi}{\partial t} + \Gamma \right) dV. \end{aligned} \quad (\text{B11})$$

In section 8.1 we assume a simplified scenario where no gas is ‘removed’ to form stars and BDM in the proto-halo. We also assume that the gas pressure and viscosity at the boundary of the proto-halo are negligible. If V is the volume occupied by gas in the proto-halo, then the surface integral above vanishes. Substituting $3kT/(2\mu m_H)$ for ϵ and using the definition of E_{gas} (equation 14), we obtain the result

$$\frac{dE_{\text{gas}}}{dt} = \frac{1}{M_{\text{gas}}} \int_V \left(\rho_g \frac{\partial \phi}{\partial t} + \Gamma \right) dV. \quad (\text{B12})$$

In sections 8.2 to 8.4, we follow the gas in the proto-halo in more detail, defining the proto-gas halo to include only gas that eventually belongs to the virialized gas halo. Thus the mass of the proto-gas halo is constant with time. The volume, V , that it occupies is irregular at early times, containing ‘pockets’ of gas which are excluded from the proto-gas halo because they later convert into stars or BDM. Using $e_{\text{gas}} = (\epsilon + \frac{1}{2} \mathbf{v}^2 + \phi)$ and $dm = \rho_{\text{gas}} dV$, we rewrite equation B11 as

$$\frac{d}{dt} \int e_{\text{gas}} dm = \int (-P\mathbf{v} + \mathbf{T}\mathbf{v}) \cdot d\mathbf{A} + \int_V \left(\rho_g \frac{\partial \phi}{\partial t} + \Gamma \right) dV, \quad (\text{B13})$$

where $\int e_{\text{gas}} dm$ is the total energy of the proto-gas halo. The surface integral gives the rate at which the proto-gas halo does work on neighbouring gas. In section 8 we investigate the pressure term only.

APPENDIX C: THE EVOLUTION OF $E_{\text{GAS,G}}$

Below, we obtain a simple expression for the variation of $E_{\text{gas,G}}$ with time, where the subscript ‘G’ means that the system evolves in the absence of non-gravitational processes. If the gas and dark matter have the same distribution, then $4\pi G \rho_{\text{g,G}} = f_{\text{gas}} \nabla^2 \phi$ for some constant $f_{\text{gas}} < 1$. Now, by integrating by parts twice, we obtain Green’s Theorem:

$$\int \phi \nabla^2 \dot{\phi} dV \equiv \int (\phi \nabla \dot{\phi} - \dot{\phi} \nabla \phi) \cdot d\mathbf{A} + \int \dot{\phi} \nabla^2 \phi dV, \quad (\text{C1})$$

where $\dot{\phi} = \partial \phi / \partial t$. If the integrals are made over all space and ϕ vanishes at infinity, then the surface integrals vanish. Since $\rho_{\text{g,G}} \propto \nabla^2 \phi$, it follows that

$$\int \rho_{\text{g,G}} \frac{\partial \phi}{\partial t} dV = \frac{\partial}{\partial t} \int \frac{1}{2} \rho_{\text{g,G}} \phi dV. \quad (\text{C2})$$

In order to substitute into equation B12, where the integration is made over the volume of the proto-halo only, we need to assume that $\rho_{\text{g,G}} = \rho_{\text{tot}} = 0$ outside the proto-halo. The volume of integration above can then be shrunk down to the proto-halo. Setting $\Gamma = 0$, equation B12 gives

$$\frac{dE_{\text{gas,G}}}{dt} = \frac{1}{M_{\text{gas}}} \frac{d}{dt} \int \frac{1}{2} \rho_{\text{g,G}} \phi dV. \quad (\text{C3})$$

Therefore,

$$E_{\text{gas,G}} = \frac{1}{M_{\text{gas}}} \int \frac{1}{2} \rho_{\text{g,G}} \phi dV + \text{constant}. \quad (\text{C4})$$